Journal of Translational Medicine

RESEARCH

Open Access

Injectable nanocomposite hydrogel for localized precision delivery of dexamethasone after traumatic brain injury: dual modulation of neuroinflammation and blood-brain barrier restoration

Bin Zhang[1†], Miao Bai[2†], Mengshi Yang[1], Yumei Wang[1], Xiyu Chen[1], Baiyun Liu[3*] and Guangzhi Shi[1*]

Abstract

Background Glucocorticoids (GCs) have been widely used in the treatment of severe traumatic brain injury (TBI) to inhibit neuroinflammation and alleviating brain edema and cannot be replaced by other drugs. However, their systemic application still faces many obstacles, such as the poor blood-brain-barrier (BBB) penetration and severe side effects. Therefore, new treatment strategy or compounds are urgently needed in clinic.

Methods Herein, an injectable nanocomposite hydrogel is developed as a biofunctionalized delivery platform for intraoperative administration of dexamethasone (DEX) after TBI. By using a mice TBI model, the safety and efficacy of the nanohydrogels in treating BBB disruption, brain edema and nerve injury were evaluated after TBI.

Results The hydrogel is composed of polysaccharide matrix (carboxymethyl chitosan and oxidized dextran) and mesoporous polydopamine (MPDA) nanoparticles loaded with DEX (MPDA@DEX@gel) that could realize in situ injection, self-assembly, a high DEX loading rate and sustained release around the lesion. The MPDA@DEX@gel exhibits excellent antibacterial and hemostatic properties, good biocompatibility and antioxidation, and self-healing capability in vitro. These in vitro and in vivo results show that local application of MPDA@DEX@gel not only alleviates brain edema, promotes neuronal survival, and improves neurological function by restoring the integrity of BBB and inhibiting neuroinflammation after TBI, but also effectively avoids the peripheral and central side effects.

Conclusion Our study provides a promising treatment strategy for the rational use of GCs in patients with severe TBI.

Keywords Traumatic brain injury, Nanocomposite hydrogel, Glucocorticoids, Blood brain barrier, Brain edema

[†]Bin Zhang and Miao Bai contributed equally to this work.

*Correspondence:
Baiyun Liu
liubaiyun1212@163.com
Guangzhi Shi
shiguangzhi@bjtth.org

[1]Department of Critical Care Medicine, Beijing Tiantan Hospital, Capital Medical University, Beijing, China
[2]Department of Neurology, The First Hospital of Tsinghua University, Beijing, China
[3]Department of Neurosurgery, Beijing Tiantan Hospital, Capital Medical University, Beijing, China

© The Author(s) 2025. **Open Access** This article is licensed under a Creative Commons Attribution-NonCommercial-NoDerivatives 4.0 International License, which permits any non-commercial use, sharing, distribution and reproduction in any medium or format, as long as you give appropriate credit to the original author(s) and the source, provide a link to the Creative Commons licence, and indicate if you modified the licensed material. You do not have permission under this licence to share adapted material derived from this article or parts of it. The images or other third party material in this article are included in the article's Creative Commons licence, unless indicated otherwise in a credit line to the material. If material is not included in the article's Creative Commons licence and your intended use is not permitted by statutory regulation or exceeds the permitted use, you will need to obtain permission directly from the copyright holder. To view a copy of this licence, visit http://creativecommons.org/licenses/by-nc-nd/4.0/.

Introduction

Traumatic brain injury (TBI), which is divided into primary and secondary injury, is the leading cause of injury-related death and disability [1]. Primary injury refers to the direct mechanical damage of the neuronal cells, blood vessels and axons of the brain caused by external forces occurring at the time of the traumatic insult. In contrast, the secondary brain injury initiated by the primary injury, is a complex series of interrelated molecular processes [2]. Among the secondary injury mechanisms, neuroinflammation, blood-brain barrier (BBB) damage, brain edema, and intracranial hypertension occur in almost all severe brain injury patients and have been confirmed to be closely associated with mortality and morbidity after TBI [3–7]. For severe TBI patients with lethal increased intracranial pressure (ICP), surgical removal of necrotic brain tissue and intracranial hematoma, and even decompressive craniectomy have been effective at reducing the ICP and mortality. However, the overall beneficial effects of surgery on functional outcomes remain unclear [8], neuroinflammation and brain edema do not cease and can become even more aggravated in the days and even weeks after surgery, leading to a range of problems and even reoperation.

Therefore, many agents that inhibit inflammation, protect BBB and alleviate brain edema have been used to improve prognosis after brain injury [9–11]. As potent anti-inflammatory agents, glucocorticoids (GCs), especially synthetic GCs such as dexamethasone (DEX) and methylprednisolone (MP) have been widely used in patients with brain tumors and other neurosurgical interventions, including severe TBI. Clear beneficial effects of GCs have been reported to alleviate edema in brain tumors, inflammatory brain disorders, and spinal cord injury via anti-inflammation and protecting BBB [12–14]. However, subsequent clinical studies did not find overall beneficial effects of GCs for severe TBI. Moreover, one clinical trial reported that the administration of high-dose MP increased the mortality of patients with severe TBI, and increased systemic infectious complications might be one possible explanation [15, 16]. Besides the peripheral side effects, we previously reported that hypothalamic-pituitary-adrenal (HPA) axis dysfunction and corticosteroid insufficiency induced by high dose synthetic GCs were closely associated with increased mortality in mice after severe TBI [17, 18]. Additionally, unlike endogenous GCs (corticosterone/cortisol), synthetic GCs poorly penetrate the BBB, even when administered at a moderate dose. A low drug concentration in brain tissue is also a possible mechanism for the failure of GCS treatment for TBI [19, 20]. However, there are currently no effective clinical therapeutic drugs that can replace GCs to inhibit inflammation and control brain edema in the acute phase after TBI. Therefore, we speculated that intraoperative local administration of DEX could bypass the BBB, effectively increase the concentration of DEX, and avoid peripheral and central side effects, potentially being the most rational way of GCs administration for severe TBI patients requiring surgery.

As smart biomaterial scaffolds with high water content, hydrogels have attracted considerable attention in biomedical engineering and pharmaceutical applications owing to their superb biomechanical properties, superior biocompatibility and good biodegradability [21, 22]. Injectable hydrogels, which can gelatinize in situ and fully fill the irregular lesion cavities in the injured brain and spinal cord, have been widely applied as supporting matrix and drug delivery platforms to promote brain tissue repair in experimental TBI models [23–25]. The three-dimensional and porous structures enable hydrogels to be suitable drug delivery devices and provide a scaffold with a favorable microenvironment for brain tissue repair. However, the low mechanical strength, weak controllability and other disadvantages of conventional hydrogels limit their applications [26, 27]. In addition, hydrogels cannot efficiently encapsulate hydrophobic drugs and control their release at the injury site, causing uncontrolled burst release and reducing the therapeutic efficiency and safety of the drugs [28]. Therefore, less hydrogels are clinically applied after brain injury. So, a method to modify hydrogel is urgently needed to avoid their shortcomings and improve their therapeutic effects.

Nanoparticles have been reported as efficient carriers of both hydrophilic and hydrophobic bioactive molecules and drugs with high biomolecule loading capacity. The mechanical and chemical properties and drug-loading capacity of hydrogels can be dramatically improved by adding nanoparticles [29]. Therefore, nanocomposite hydrogels are excellent supporting matrices for tissue repair and carriers for local drug administration. In the present study, to avoid shortcomings, improve the mechanical properties and increase the drug loading efficiency of hydrogel, we developed an injectable nanoarchitecture-integrated hydrogel delivery platform for the intraoperative administration of dexamethasone after TBI. The hydrogel was composed of polysaccharide matrix (carboxymethyl chitosan, CMC; and oxidized dextran, OD) and mesoporous polydopamine (MPDA) nanoparticles (NPs) loaded with dexamethasone (MPDA@DEX@gel). To improve the antibacterial and hemostatic properties of hydrogel, antiseptic quaternary ammonium salts and hemostatic polypeptides were grafted onto chitosan and dextran. The MPDA@DEX@gel system possessed good biocompatibility and biodegradability, and could realize in situ injection, self-assembly, a high loading capacity and sustained release of DEX in the irregular lesion cavity. We hypothesized that the local application of the MPDA@DEX@gel not only

alleviated brain edema, promoted neuronal survival, and improved neurological function by restoring the integrity of BBB and inhibiting neuroinflammation, but also effectively avoided the peripheral and central side effects.

Materials and methods

Chemicals and reagents

N,N-Dimethyldodecylamine, carboxymethyl chitosan, ethylene glycol, epoxy chloropropane, ethanol, glutaraldehyde and sodium periodate were purchased from Aladdin Biochemical Technology Inc (Shanghai, China). Glucan was purchased from Macklin Biochemical Technology Inc (Shanghai, China). RADARGDK was supplied by GL Biochem Ltd (Shanghai, China). Dopamine hydrochloride and dexamethasone were purchased from Sigma (Germany). Cell Counting Kit (CCK)-8 and 2′,7′ -dichlorofluorescein diacetate (DCFH-DA) were obtained from Beyotime Institute of Biotechnology (Nantong, China).

Preparation and characterization of MPDA@DEX nanoparticles

Mesoporous PDA NPs were synthesized using Pluronic F-127 and 1,3, 5-tritylene (TMB) as organic template. Briefly, pluronic F127 (200 mg) was uniformly dissolved in the mixture of ethanol (10 ml) and water (10 ml), and then 1,3,5-trimethylbenzene (0.2 ml) was added and stirred until uniformly dispersed. At last, ammonia (1 ml) and dopamine (100 mg) were added to the mixture and stirred at room temperature for 4 h, and then centrifuged three times. and MPDA was obtained after removing the template.

For preparation of MPDA@DEX, DEX was dissolved in ethanol to obtain a 0.5 mg/mL DEX solution. The DEX solution was then mixed with the MPDA NPs (3 mg/mL) at a volume ratio of DEX: MPDA = 3:1. The mixture was stirred at room temperature for 24 h, centrifuged at 13500r/min for 10 min, and then washed 3 times to obtain MPDA@DEX NPs. The size and zeta potential of MPDA@DEX NPs were determined via dynamic light scattering method (DLS, Zetasizer Nano ZS90, British Malvern). The morphology of the MPDA@DEX NPs was characterized via transmission electron microscopy (TEM, FEI Tecnai G2 F20 S-Twin Jeol, American FEI).

In accordance with a previous study [5], the DEX loading capacity of MPDA NPs was quantified by HPLC. First, a standard curve was created by testing the peak area of different concentrations of DEX. Then, DEX (0.5 mg) was mixed with MPDA NPs (1 mg) and incubated for 24 h. After centrifugation for 10 min at 13,500 r/min, a HPLC was used to measure the peak area of DEX in the supernatant. Finally, the DEX loading capacity was calculated.

Preparation and characterization of Schiff-base hydrogels

0.01mmol dimethyldodecyl tertiary amine solution and 0.04mmol epichlorohydrin solution were mixed at 80 ℃ for 1 h. After the mixture changed from transparent to dark yellow, the reaction products were precipitated with ether and centrifuged to obtain crude EPDMDAC (EPD). The crude EPD was ultrasonically washed 3 times with ether, and then dried and purified in vacuum. EPD (30 mg) was added to CMC (3%, 5 ml) solution for 4 h, followed by dialysis for 24 h with a 1000 KDa dialysis bag to obtain EPD-CMC.

OD was synthesized by oxidizing dextran with sodium periodate. Briefly, dextran (5 g) was dissolved in deionized water (250 mL) to form a dextran solution. Sodium periodate dissolved in deionized water (5 mL) was added dropwise to the dextran solution. The mixture was subsequently stirred at 37 °C at room temperature in the dark for 3.5 h. Then, 3 mL of glycol was added to the mixture to stop the oxidation reaction, and the mixture was stirred for 1 h. The product was dialyzed in distilled water (MWCO 1400 Da) for 3 days and lyophilized to obtain OD. To synthesize RAD-OD, the hemostatic peptide RADARGDK (RAD, 10 mg) was added to glucan oxide solution (5%, 5 ml) and reacted for 2 h though Schiff-base reaction.

Finally, the EPD-CMC solution (2%) and RAD-OD solution (5%) were mixed at a volume ratio of 1:3 to obtain control blank hydrogel. To obtain the MPDA@DEX NPs hydrogel, the MPDA@DEX solution was added to an equal volume of EPD-CMC solution and mixed with RAD-OD at a volume ratio of 2:3. The mixture gradually became a colloid after mixing for 30 s.

The morphological properties of the samples were observed with Tecnai G2 F20 S-Twin transmission electron microscope (TEM, FEI, American) and scanning electron microscope (apreo2c, Thermo, American). Tensor II Fourier transform infrared (FTIR) spectrometer (Nicolet iS 10, Thermo-Fisher Co., USA) was used to determine the chemical groups of the hydrogels. The crystal structure was measured via the X-ray diffractometer (XRD, Ultima IV, Japan). The contents of carbon, nitrogen, oxygen and chlorine on the surface of the material were measured via X-ray photoelectron spectroscopy (XPS) (ESCALAB 250XI, Thermo, USA).

For the swelling test, the hydrogels were freeze-dried, and the initial weight of each hydrogel was recorded as W0. The hydrogels were submerged in PBS at 37 °C for 48 h until they were fully swollen. The hydrogels were weighed at specific time points until the mass remained constant. The excessive surface water was gently wiped dry with wet filter paper and the weight of the swollen hydrogel was measured as Wt. The swelling ratio was calculated as follows: swelling ratio = (W1−W0)/W1 × 100%.

The degradation of the hydrogels were evaluated by submerging the hydrogel with a constant weight (W0) into PBS. After being incubated at 37 °C for different durations, the hydrogels were removed and the surface water was gently wiped dry with absorbent paper and weighed (Wt). The degradation ratio was calculated as: (W0-Wt)/W0 × 100%.

TGA2 SF/1100 (Mettler-Toledo, Switzerland) was used to conduct thermogravimetric analysis (TGA) of hydrogels (5 mg per sample) under air and nitrogen atmosphere (30 to 700 °C, heating rate = 10 °C /min).

The hydrogel rheology (20 mm in diameter, 2 mm in height) was analyzed using MARS 60 rheometer (Haake, Germany). The storage modulus G′ and loss modulus G′′ were measured via sweep frequency tests at 25 °C. Strain amplitude sweep ($\gamma = 0.1 - 1000\%$) tests were conducted on the hydrogel samples at 25 °C to obtain the linear viscoelastic region. Then, alternate step strain sweep test was performed with the amplitude strains switched from low strain (1%) to high strain (300%) and with a duration of 100 s for each strain. A cut/heal test was also conducted to investigate the macroscopic self-healing behavior of the hydrogel. According to ASTMD882-12 standards, hydrogels (10 mm diameter, 10 mm high) were subjected to compression tests using 20 N load cell at 120 mm with a clamping distance of 1 cm.

In vitro drug release study

In vitro release tests of DEX from MPDA@DEX, DEX@gel (2 h, 4 h, 6 h, 8 h, 12 h, 24 h) and MPDA@DEX@gel (3 h, 6 h, 8 h, 12 h, 24 h,48 h, 3 days, 5 days, and 7 days) were performed using 200 μl of hydrogel. PBS (3 ml) was added to the hydrogel samples and 100 ul of soaking solution were taken from each sample at different time points. The concentrations of DEX were tested via high-performance liquid chromatography (HPLC, Waters e2695, USA).

In vitro antibacterial experiments

The agar diffusion method was used to assess the antibacterial properties of the hydrogels in vitro. *Staphylococcus aureus* (*S. aureus*, ATCC6538) or *Escherichia coli* (*E. coli*, ATCC25922) solution was added to the Luria Bertani (LB, Shanghai Yuanye Bio.Technology Co., Ltd.) solid medium. The antimicrobial peptides were diluted to 5, 10, 15, 20, 30, 40, 50 and 75 mg/mL, and the suspensions were taken at 150 rpm at 37 ℃. The minimum inhibitory concentration (MIC) was evaluated according to the minimum antibacterial agent concentration for 24 h to inhibit bacterial growth. The bacteria group without antibacterial agent was the positive control group. The disc-shaped hydrogels (diameter = 1 cm, weight = 0.2 g) were attached to the surface of the solid medium, which were then placed in a 37 °C constant temperature incubator. The inhibition zones were observed after 24 h incubation to verify the antibacterial effect.

In vivo hemostatic performance

Adult SD rats (male, 200–220 g, Beijing Vital River Experimental Animals Technology, Ltd., Beijing, China) were subjected to liver injury modeling ($n = 3$) and tail amputation ($n = 3$) to evaluate the hemostatic properties of the hydrogels. The rats were anesthetized with 2% pentobarbital and then fixed on a corkboard. The rat tail was cut in the middle with surgical scissors and the liver surface was incised. The bleeding site was immediately covered with 500 μL of hydrogel. The hemostatic time and the amount of blood loss were recorded. All experimental procedures were approved by the Capital Medical University Institutional Animal Care and Use Committee.

The whole-blood clotting test was performed according to the established procedure [31]. Briefly, CaCl2 (0.2 M, 30 ul) was added to a mixture of whole blood (0.4 ml) and citrated (0.04 ml, 38 mg/ml) and then injected into each hydrogel sample in a centrifuge tube. After incubation for 2 min at 37 °C, deionized water (10 mL) was added to the tube and incubated for another 5 min, after which the supernatant was collected and centrifuged. The absorbance values were recorded (B). The absorbance of whole blood in deionized water (10 mL) was used as a negative control (A). The blood clotting index (BCI) was calculated as BCI (%) = A/B × 100%.

In vivo and in vitro biocompatibility

BV2 cells were provided by Procell Life Science & Technology Co., Ltd. (Wuhan, China, CL-0493) and cultured in MEM (Procell Life Science & Technology Co., Ltd., CM0493). The cultures were maintained at 37 °C in a humidified atmosphere with 5% CO_2 and subsequently utilized for immunofluorescence staining.

In the present study, a CCK-8 staining assay was used to evaluate the in vitro biocompatibility of the hydrogels. Briefly, BV2 cells were incubated at 37 °C for 24 h, and the culture medium was replaced with fresh culture medium containing 10 μl hydrogels. After further incubation for 2, 4, 6, 8, 12, and 24 h, then CCK-8 (10%) was added to the replaced culture medium, and the mixture was incubated for another 4 h. The OD value at 450 nm was measured by an ultraviolet spectrophotometer (Uv-2600i, SHIMADZU, Japan). Cell viability = A1/A0 × 100%. where A1and A0 were the absorbance value of the treated group and the control group, respectively.

To assess in vivo biocompatibility, organs (heart, liver, spleen, lung, and kidney) and blood from experimental mice were obtained from the same mice as those from which brain sections were collected on postinjury day 7 after the hydrogels were injected in situ into the surgical area in the brain. Hematoxylin and eosin (H&E) staining

was used to assess histological change. In addition, the liver and kidney functions were evaluated by testing the levels of alanine aminotransferase (ALT), aspartate aminotransferase (AST), creatinine (CREA), and blood urea nitrogen (BUN) via ELISA assay.

ROS assay

A ROS test kit (Beyotime, Shanghai, China) was used to assess the intracellular ROS levels. According to the manufacturer's procedures, BV2 cells were incubated overnight, and the medium was changed with fresh culture medium containing 10 μl hydrogels for 4 h. Next, DCFH-DA and DAPI were added to culture medium and incubated for 30 min to reveal the ROS level. Fluorescence images were captured using a confocal laser scanning microscope (A1, Nikon, Japan).

BV2 cells were devided into the following four groups: (1) the control group; (2) the LPS group, in which cells treated with LPS; (3) the MPDA@gel group, in which LPS-induced cells were treated with MPDA@gel; and (4) the MPDA@DEX@gel, in which LPS-induced cells were treated with MPDA@DEX@gel. In the lipopolysaccharide (LPS, Sigma, L4391) group, LPS (1 μg/ml) was used to stimulate BV2 cells.

Controlled cortical impact (CCI) animal models

Adult male C57BL/6 mice (20–22 g, Beijing Vital River Experimental Animals Technology, Ltd., Beijing, China) were used in this study. All experimental procedures were approved by the Capital Medical University Institutional Animal Care and Use Committee.

A severe TBI model was established with a PCI3000 PinPoint Precision Cortical Impactor (Hatteras Instruments, Cary, NC, USA) as we previously described [20]. Briefly, each mouse was anesthetized with continuous 2% isoflurane and fixed on a stereotaxic frame (RWD Life Science Co., Shenzhen, Guangdong, China). The skull was fully exposed by a midline incision, and a right craniotomy (4 mm in diameter) was performed midway between the bregma and lambda with the underlying dura intact. The impact injury was induced with a 3-mm circular impact tip using the impact parameters described previously (velocity: 3.5 m/s; compression time: 400 ms; and depth: 2 mm). Craniotomy without CCI was conducted in rats of Sham group. A thermal pad was used to maintain the body temperature throughout the surgical procedures.

Experimental groups and treatments

The mice were randomly divided into the following groups: (1) the sham group; (2) the CCI group; (3) the MPDA@gel treatment group, and (4) the MPDA@DEX@gel treatment group. For the mice in the MPDA@gel and MPDA@DEX@gel groups, 50 μL of hydrogels (with a DEX concentration 0.5 mg/ml Gel) were injected in situ into the surgical area. The DEX dose was chosen based on our pilot experiments and previous studies [18].

Detection of DEX, corticosterone, and inflammatory factors

To test the plasma levels of corticosterone and inflammatory factors (TNF-α, IL-1 β, IL-6), blood samples (1 ml) were collected transcardially on day 3 after TBI. Plasma was separated and stored at -80 °C. In addition, Inflammatory factors in the ipislateral hemisphere were also detected. The cell fragments were removed by centrifugation at 13,000 rpm for 20 min at 4 °C. The ipsilateral hippocampus and pituitary were collected on the postinjury day 3. After the samples had been homogenized, each supernatant was collected. DEX was evaluated by HPLC, and corticosterone and cytokine levels were detected using mouse ELISA kits (Nanjing KeyGen Biotech. Co., Ltd.).

Immunofluorescence staining in vivo and vitro

Immunofluorescence staining was performed at 3 and 7 days after TBI. Brain slices ($n = 6$) were single-stained (NEUN) or double-stained (CD16/32 + Iba-1) for immunohistochemical evaluation according to our previous procedures. For in vitro immunofuorescence analysis, BV2 cells were plated on coverslips in a 6-well cell culture plate. After treatment, primary microglia were fixed with 4% paraformaldehyde (PFA) for 20 min and then incubated in distilled water containing 10% goat serum and 0.1% Triton X-100 for 1 h to permeabilize the cells and block nonspecific protein-protein interactions. The brain slice and cells were incubated with primary antibodies overnight at 4 °C. Alexa Fluor 488 (1:500, ab150113, Abcam, UK) or 594 (1:500, ab150080, Abcam, UK) -conjugated secondary antibodies were then added and incubated for 1 h at room temperature. Antibodies are listed as follows: rabbit polyclonal anti-NeuN (1:200, Abcam, ab177487, UK), anti-CD16/32 (1:500, Abcam, ab223200, UK), and anti-Iba-1(1:200, Abcam, ab178846, UK), DAPI (Sigma-Aldrich, St. Louis, MO) for 10 min. The number of microglia, neurons in the perilesional cortex or ipsilateral hippocampus were quantified as previously described [18].

Determination of brain water content

The wet and dry weights of the brains were recorded to evaluate the brain water content 3 days after TBI. Mouse brain tissue was removed without transcardial perfusion, and the injured cerebral hemisphere was subsequently dissected and weighed (wet weight). The tissue was subsequently dried at 80 °C for 72 h until the weight was constant (recorded as dry weight). The percentage of brain water content was calculated via the following formula:

brain water content (%) = (wet weight-dry weight)/wet weight×100%.

Evans blue extravasation

The permeability of the BBB was assessed by testing the extravasation of Evans blue (EB, Sigma) into the injured hemisphere after TBI. EB solution (4%, 3 mL/kg) was injected through the mouse tail vein. Four hours later, the animals were anesthetized and transcardially perfused with PBS. The injured hemisphere was dissected and weighed, and subsequently homogenized in formamide at 72 °C for 3 days. After centrifugation, the supernatant was collected and its absorption was measured at 620 nm using spectrophotometer (Bio-Rad, Hercules, CA, United States).

Western blot analysis

The cortex and hippocampus of the injured side were isolated from the mice 3 days after TBI. Total protein ($n = 6$) was extracted and the protein concentration was detected, and then western blot analysis was performed as previously described [20]. The primary antibodies used were as follows: anti-occludin (1:1,000, ab224526, Abcam, UK), anti-claudin-5 (1:1,000, ab131259, Abcam, UK), anti-ZO1 (1:1,000, ab276131, Abcam, UK), and anti-GAPDH (1:5000, ab8245, Abcam, UK) antibodies. The protein blots were developed via chemiluminescence (Bio Spectrum 500 Imaging System; UVP Co., Upland, CA, USA). ImageJ software (version 1.49) was used to quantify the relative band density.

Neurological function assessment

The modified neurological severity score (mNSS) is widely used to comprehensively evaluate the motor, sensory, balance and reflex functions after TBI model. In the present study, the mNSS were performed on postinjury Days 1, 3, 7 and 14. The morris water maze (MWM) test was performed to evaluate spatial learning ability as we described previously [18]. Each mouse underwent 4 trials per day for 5 consecutive days (8–12 days after CCI) to find the platform submerged below the water. Twenty-four hours after training, the hidden platform was removed, and a probe trial was conducted. The goal quadrant time and distance were recorded by a video tracking system.

Statistical analysis

All the data are presented as the means ± standard deviations (SDs). The data were analyzed using SPSS 26.0 (IBM Corporation, USA). Repeated analysis of variance (repeated ANOVA) with the Bonferroni correction was used to analyze the mNSS and MWM latency. The other results were analyzed by one-way ANOVA followed by Tukey's post hoc test. A P-value < 0.05 was considered statistically significant.

Results

Formulation and characteristics of DEX-loaded MPDA NPs

Figure 1 showed the schematic diagram of the synthesis (Fig. 1A) and intraoperative local administration of MPDA@DEX@gel in TBI (Fig. 1B).

To increase DEX-loading capacity of the hydrogel and realize a sustained release of DEX around the injury site, MPDA were synthesized and used as the carrier of DEX in this study. The particle size and zeta potential of the DEX, MPDA NPs, and MPDA@DEX were analyzed by DLS, and the morphology was observed by TEM (Fig. 2A, B). As shown in Fig. 2C, D, the average size of MPDA NPs was 155.9 ± 2.06 nm. After loading, the particle size of MPDA@DEX was increased to 167.6 ± 2.47 nm, and the polydispersity index was 0.004, which proves that it has good dispersion. In addition, Fig. 2E showed that the potential of MPDA itself was– 40.89 ± 1.30 mV and that of DEX was – 2.39 ± 0.11 mV. After loading, the potential of MPDA@DEX increased to -36.69 ± 0.98 mV. Both the potential and particle size of MPDA changed significantly after DEX loading, which illustrated the successful preparation of MPDA@DEX. The value of the hydrated particle size larger than that observed via TEM can be attributed to the formation of a thicker hydrated layer on its surface.

Infrared spectroscopy was used to analyze the changes in the components of MPDA after DEX loading. Figure 2G shows that MPDA has three characteristic absorption peak at 2969 cm^{-1}, 1617 cm^{-1} and 1290 cm^{-1}, respectively attributed to the stretching and bending vibration absorption peaks of C-H, the characteristic skeleton vibration peak of aromatic ring, and the stretching vibration absorption peak of phenolic C – O. DEX had stretching vibration peaks at 1704 and 1662 cm-1 for -C = O connected between C3 ring and C20 carbonyl, and a characteristic absorption peak at 1618 cm-1 for the double bond framework conjugated to -C = O. In addition, the stretching and bending vibration absorption peaks of O-H and C-F were also found at 3472 cm-1 and 1271 cm-1 respectively in DEX. After DEX loading, the characteristic stretching vibration absorption peaks of DEX in MPDA@DEX were found at 1705, 1619 cm-1 and 1663 cm-1for the -C = O bond. The characteristic absorption peak in the ultraviolet spectrum and the mass loss rate in the TG of MPDA@DEX further indicated the successful loading of DEX on MPDA. The drug loading rate was evaluated by testing the supernatant DEX using HPLC. The loading rate of DEX in MPDA@DEX was 29.49% ± 0.28%.

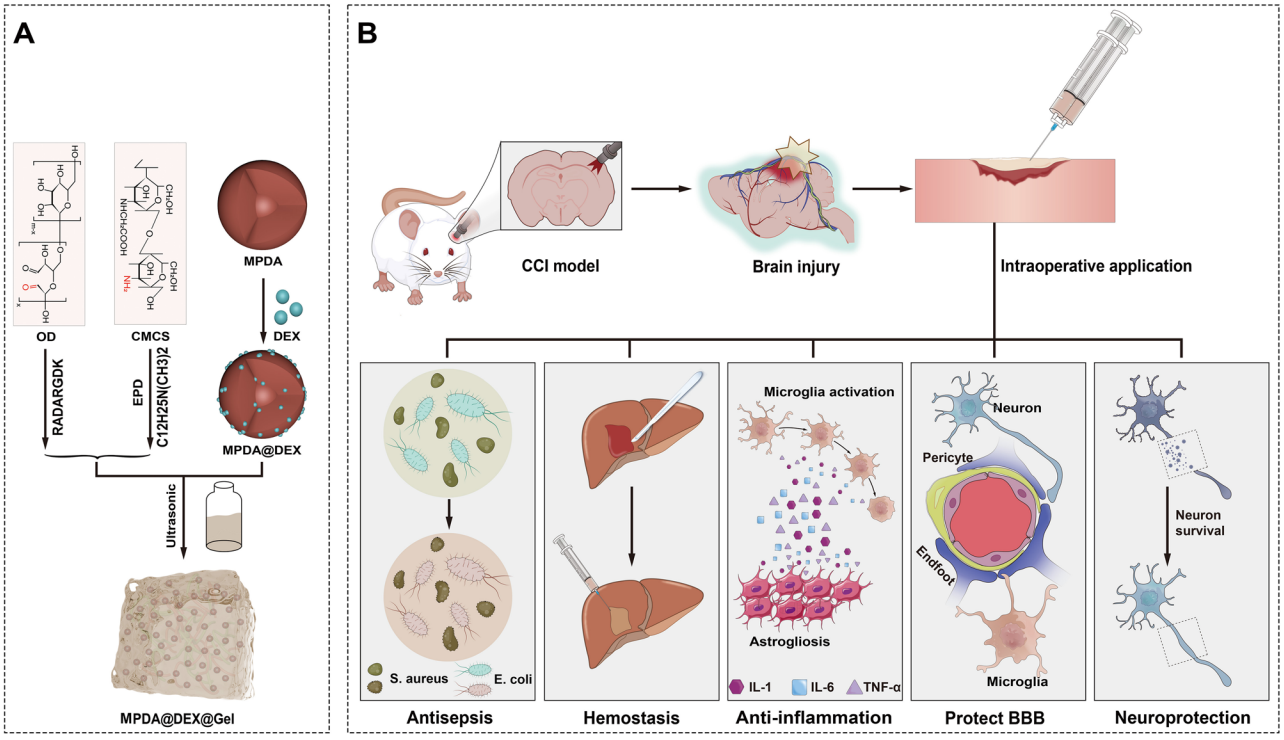

Fig. 1 Schematic diagram of the synthesis and intraoperative local administration of MPDA@DEX@gel in TBI. (**A**) illustration of the synthesis and characteristics of MPDA@DEX@gel; (**B**) intraoperative local administration of MPDA@DEX@gel. MPDA@DEX@gel exerts neuroprotective effects by anti-neuroinflammation, protect BBB and reduced brain edema after TBI

Synthesis and characteristics of the hydrogels

In the present study, to achieve local application of MPDA@DEX NPs, we developed an injectable, self-healing, and in situ cross-linked hydrogel system with enhanced antibacterial and hemostatic properties based on carboxymethyl chitosan and oxidized dextran. Additionally, to enhance the antibacterial and hemostatic properties of the hydrogel, CMC was first grafted with antiseptic quaternary ammonium salt (EPD-CMC) and then OD was grafted with hemostatic polypeptide (RAD-OD). Finally, EPD-CMC cross-linked with RAD-OD via an aldehyde-amine Schiff-base reaction to construct the EPD-CMC/RAD-OD hydrogel. MPDA@DEX@EPD-CMC/RAD-OD hydrogel (MPDA@DEX@gel) with antibacterial, hemostatic, and controlled release functions was obtained.

The micromorphology of the hydrogels was observed by scanning electron microscopy (SEM). As shown in Fig. 2I, the hydrogels presented a crosslinked three-dimensional network structure. Compared with those in blank gels, particles of approximately 70–300 nm in size were observed in both MPDA@DEX@gel group, suggesting that the hybrid nanoparticles were successfully loaded into the gel.

The FTIR results showed that the peak of OD grafted with the hemostatic polypeptide at 3300 cm-1 was significantly widened compared with that of OD alone, which might be attributed to the appearance of -NH vibration peak in the hemostatic polypeptide. In addition, compared with CMC alone, EPD-CMC presented a new absorption peak at 1471 cm-1 attributed to the methyl group of ammonium, which illustrated the formation of N-(2-hydroxyl, 3-trimethylamine) -propyl chitosan • trichloride under -NH2. The above results illustrated the successful preparation of EPD-CMC and RAD-OD (Fig. 2J, K).

In addition, the elements on the surface of the material were further analyzed by X-ray electron spectroscopy. As shown in Fig. 2N-Q, the results of the full spectrum of elements revealed that the elements of hydrogel without antibacterial agent (CMC /RAD-OD) were mainly C, O and N, whereas the hydrogel with the antibacterial agent (EPD-CMC/RAD-OD) contained four elements: C, O, N, and Cl, indicating that the antibacterial agent was successfully incorporated.

Subsequently, TGA test was performed to assess the thermal stability of the designed hydrogels. As shown in Fig. 2H, there was a slight reduction in mass below 150 °C, which was probably attributed to the evaporation of internal water contained in the hydrogels. The MPDA was gradually decomposed as the temperature increased from 150 °C to 790 °C. Additionally, DEX is relatively stable below 260℃, and there was basically no reduction in weight. However, when the temperature was above 260

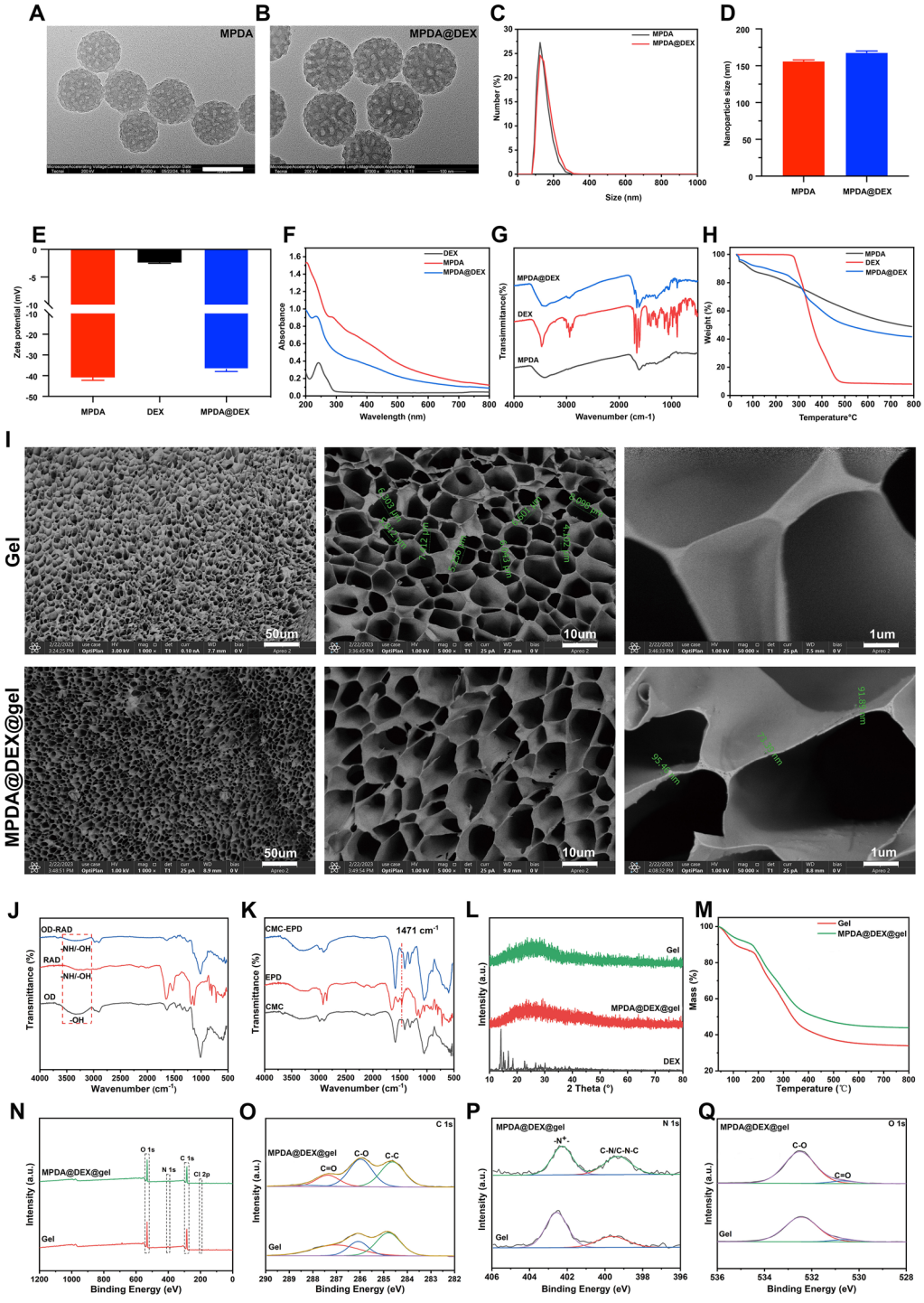

Fig. 2 Synthesis and characterization of MPDA@DEX and MPDA@DEX@gel. (**A**, **B**) TEM images of MPDA and MPDA@DEX (Scale bar: 100 nm); (**C**, **D**) Size distribution of MPDA and MPDA@DEX; (**E**) Zeta potential of MPDA, DEX and MPDA@DEX; (**F**) UV-Vis spectra of MPDA、DEX and MPDA@DEX; (**G**) FTIR spectra of MPDA, DEX and MPDA@DEX; (**H**) TG analysis of MPDA, DEX, MPDA@DEX; (**I**) SEM images of Gel and MPDA@DEX@gel; (**G**) FI-TR of OD, RAD and OD-RAD; (**K**) FI-TR of CMC, EPD and CMC-CPD; (**L**) XRD of Gel and MPDA@DEX@gel; (**M**) TG curves of gel and MPDA@DEX@gel; (**N**-**Q**) XPS Gel and MPDA@DEX@gel. Data are presented as means ± SD ($n = 3$)

℃, DEX began to undergo thermal decomposition, and the weight loss was about 89.838% when the temperature reached 400 ℃. Compared with the that of MPDA, the weight loss of MPDA@DEX was about 7.22% at 150–480 ℃, which mainly due to the decomposition of DEX coated on the MPDA NPs. At 790 ℃, the residual weight ratio of blank Gel and MPDA@DEX@gel in the air environment were 30% and 44% respectively (Fig. 2M). The results revealed that the thermal stability of the hydrogel significantly enhanced after the addition of MPDA@DEX.

The in vitro degradation behavior of the hydrogels was then evaluated through incubation in PBS. As shown in Fig. 3A-C, the hydrogels were quickly formed via Schiff-base reaction after EPD-CMC and RAD-OD were fully mixed. The morphology and weight of the wet hydrogels soaked in PBS were nearly unaltered in the first 24 h. Subsequently, the hydrogel structure began to collapse. Finally, the hydrogel was degraded into little pieces over time and almost completely disappeared. After being incubated for 28 days, the blank Gel and MPDA@DEX@gel presented 84% and 75% mass loss in PBS, respectively (Fig. 3D). Moreover, MPDA@DEX@gel exhibited a relatively slower degradation rate as compared to that of the blank Gel. The possible reason might be that the addition of MPDA increased the number of Schiff-base reaction sites and promoted the internal cross-linking of the hydrogel.

Swelling without dissolving is an important characteristic of hydrogels. The water uptake and retention capacities of the hydrogels were evaluated by testing the swelling ratios at different time points. As shown in Fig. 3E, the water uptake of blank Gel and MPDA@DEX@gel were dramatically increased in the first 10 s, then became slowly and steadily. The final swelling ratio of blank Gel and MPDA@DEX@gel was 1700% and 1650%, respectively.

HPLC was used to detect DEX release from MPDA, DEX@gel, and MPDA@DEX@gel. As shown in Fig. 3F, G, DEX release from MPDA@DEX is at approximately 70.2% within 24 h. an uncontrolled burst release of DEX was found in the DEX@gel group, and more than 90% of DEX was released within 8 h. In contrast, the release of DEX from the MPDA@DEX@gel was continuous and controlled, and more than 80% of the drug was released by day 7.

The rheological characteristics of the different hydrogels were evaluated. We found that the hydrogel generated with CMC and OD at a ratio of 1:3 had the largest G' and G" and was therefore selected for the subsequent experiments. As shown in Fig. 3H, the G′ values were always greater than the G′′ values without oscillatory strain. However, with the increase of strain, the G′ decreased continuously, and the G′ ′ gradually increased. When the strain amplitude increased to approximately 100%, the intersection of G′ and G′′ occurred, and then the G′′ started to exceed the G′ indicating that the hydrogel state began to change from elasticity to fluidity. Finally, G′ dropped dramatically as the strain continuously increase, indicating that the gel structure collapsed and became a fluid-like state at this time. Interestingly, with the addition of MPDA nanoparticles, G 'of the gel was gradually increased, suggesting a more stable internal structure of the gel. The possible reason might be that hydroxyl group of MPDA increases the number of hydrogen bonds and the Schiff base reaction sites. In addition, Fig. 3I showed that the viscosity of both the blank hydrogels and MPDA@DEX@gel gradually decreased as the shear rate continued to increase with a constant shear strain, which was the typical shear-thinning features, indicating good injectability of hydrogels.

Afterward, the self-recovery properties of hydrogels were assessed. As shown Fig. 3J, the results of dynamic stepwise strain amplitude tests (100 s interval) showed that G′ dropped dramatically and was lower than G′′ when the value of shear strain switched from 1 to 300%, indicating that the hydrogel transformed from a stable hydrogel network into a sol state. Interestingly, the G′ and G′′ were restored rapidly to their initial values after the strain was switched to 1% again, suggesting the reconstruction of the ruptured hydrogel network. Moreover, this gel-sol transition process can be repeated steadily even after several cycles, suggesting the excellent self-recovery properties of the hydrogels.

In addition, the cut/heal test revealed that after the four differently colored hydrogels were put together for 1 h, the dyes at the damaged interface obviously fused and the cuts completely healed without any intervention (Fig. 3K). In summary, the above results proved that MPDA@DEX@gel had excellent injectability, in situ gelatinization, and self-healing properties, which were helpful for intraoperative application to fill the irregular lesion cavities in the injured brain after TBI.

The compressive stress-strain test and curves were shown in Fig. 3L, M, the hydrogel with CMC and OD at the ratio of 1:3 withstood compression without breaking, and after compression was released, the hydrogels recovered rapidly to their initial shape.

The compression property of gel gradually decreased with the increase of OD content. The adhesive properties of the gels were assessed. As shown in Fig. S1, the fresh prepared MPDA@DEX@Gels were used to adhere mouse organs (brain, heart, liver, spleen, lung, and kidney). All the organs were closely and firmly adhered to the fresh MPDA@DEX@Gels, and did not fall off when turned over the dishes, indicating the good adhesive properties of the gels.

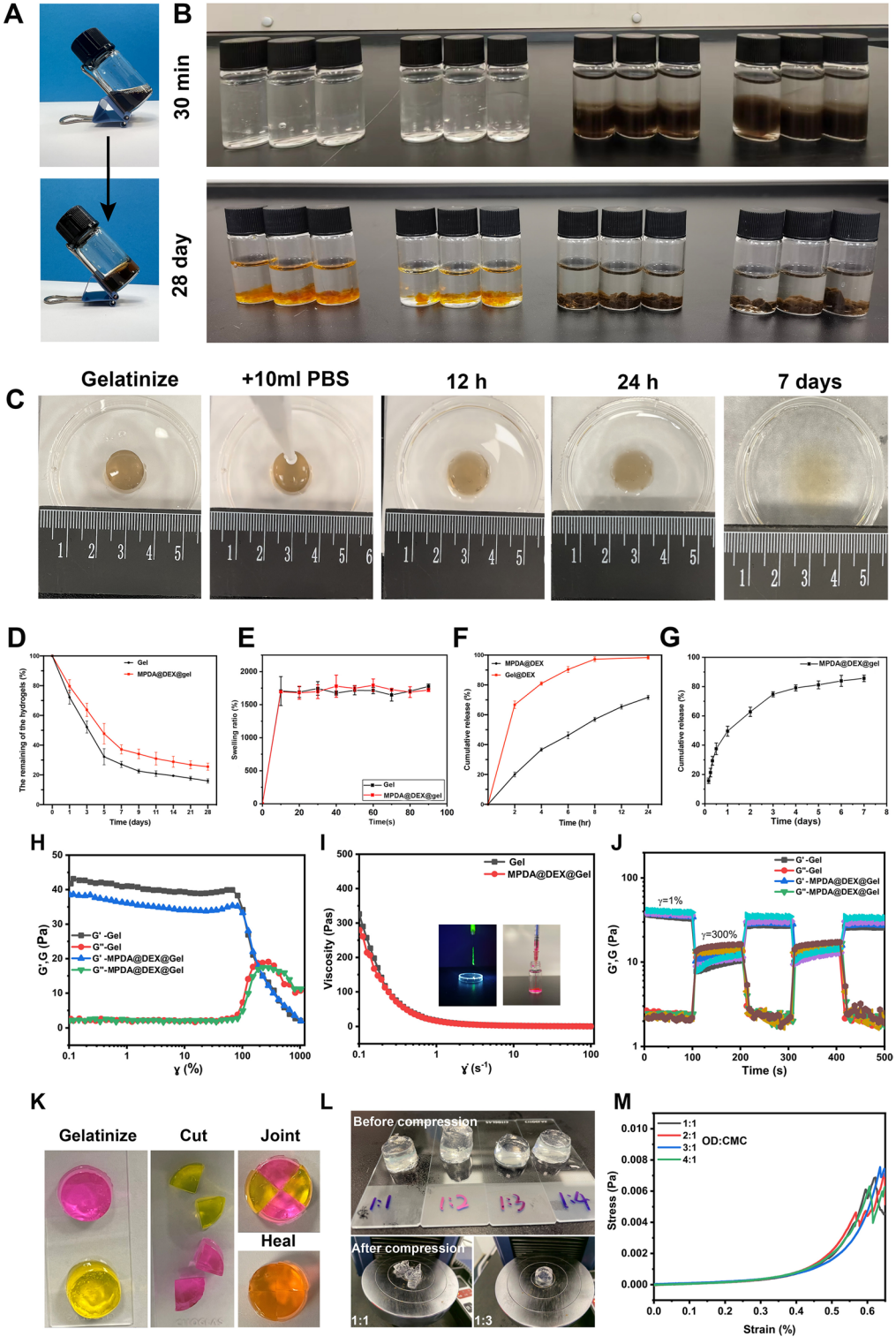

Fig. 3 The swelling ratio, drug release and rheological performances of Gel and MPDA@DEX@gel. (**A**) Demonstration of gelation; (**B**, **C**) Physical picture of gel swelling and degradation; (**D**) The degradation curve of Gel and MPDA@DEX@gel; (**E**) Swelling ratio of Gel and MPDA@DEX@gel; (**F**, **G**) Release curve of DEX from MPDA, gel, and MPDA@DEX @Gel; (**H**) evolution of G′ and G″ under different oscillation strains (ε = 1 rad/s); (**I**) viscosity of Gel, and MPDA@DEX@gel, versus shear rate (γ = 1%); (**G**) Thixotropic characterisation of self-healing Gel and MPDA@DEX@gel, at alternate strain of 1% and 300%, respectively, with angular frequency of 1 rad/s; (**K**) Integration of two broken hydrogel pieces after mutual interaction; (**L**) Before and after compression of different proportions of gels; (**M**) Uniaxial compression stress-strain curves of gels with different proportions. Data are presented as means ± SD (*n* = 3)

Antibacterial properties of the MPDA@DEX@gel in vitro

Intracranial bacterial infection is one of the most common and severe complications of intraoperative application of synthetic medical materials or heterogeneous biomaterials after craniotomy, which seriously affects the patient prognosis and even leads to reoperation. Therefore, to improve the antibacterial properties of the hydrogel, an antiseptic quaternary ammonium salt EPD was grafted with carboxymethyl chitosan. In the present study, AGAR plate diffusion and the bacteriostatic zone method was used to assess the antibacterial properties of hydrogels. S. aureus and E. coli were spread on the plates, then filter papers containing antibiotic agents at different concentrations were placed on the plates. As shown in Fig. S2A, after incubation for 24 h, antibacterial agent at 5 mg/mL showed an obvious inhibitory effect on the S. aureus plate but not on the E. coli plate. With increasing the EPD concentration, the inhibition zone was larger, and when the concentration was greater than 30 mg/mL, the inhibitory effect for S. aureus was not significantly increased, and an obvious inhibition zone was found in E. coli plate. Therefore, 30 mg/mL was selected as the optimal antibacterial concentration. As shown in Fig. S1B, both blank Gel and MPDA@DEX@gel containing antibacterial agents showed obvious antibacterial effects and the inhibitory zone of both S. aureus and E. coli were remarkably increased. The above results indicated that the addition of EPD significantly enhanced the antibacterial properties of the hydrogels.

Hemostatic properties of the MPDA@DEX@gel in vivo

In the present study, to enhance the hemostatic properties of hydrogels, the hemostatic peptide RADARGDK was grafted with carboxymethyl chitosan. Liver injury and tail amputation models and the BCI were used to evaluate the hemostatic properties of hydrogels in vitro and vivo. As shown in Fig. S3, the blank gel containing RAD significantly reduced both the bleeding mass and bleeding time in the liver injury and tail amputation models. Similarly, compared with that in the control group, the BCI was significantly lower in the blank Gel group. The addition of MPDA NPs further enhanced the hemostatic properties of the hydrogel, the bleeding mass, bleeding time, and BCI were significantly decreased in that of MPDA@DEX@gel group compared with blank Gel group, which might be attributed to the increased adhesive properties of the gel by adding MPDA NPs.

Biocompatibility and antioxidation of MPDA@DEX@gel in vitro and in vivo

To test the ROS-scavenging properties of the MPDA@gel and MPDA@DEX@gel in vitro, DCFH-DA was used to evaluate the intracellular ROS level after BV2 cells were activated by LPS. As shown in Fig. 4A, B, the ROS levels were dramatically increased in the LPS group compared with the control group. The administration of MPDA@DEX@gel significantly reduced the levels of ROS, indicating its excellent antioxidative effects.

Biocompatibility is a critical factor for the clinical application of hydrogels. In our study, CCK-8 assay was used to assess the toxicity of the hydrogels in vitro. As shown in Fig. 4C, the BV2 cell proliferation rate between different hydrogels and the control groups at different time points, indicating the excellent cytocompatibility of MPDA@DEX@gel hydrogels.

In addition, the biocompatibility of the hydrogels was also assessed in vivo. As shown in Fig. S4, no obvious pathological changes were found in the hydrogel groups compared to that in the control group, and there were not statistical differences in blood parameters (AST, ALT, CREA and BUN) among different groups, indicating good biosafety of the MPDA@DEX@gel in vivo.

DEX poorly penetrated in brain, and local administration effectively bypassed the BBB and increased the local drug concentration

To evaluate the penetration of DEX in the brain, we tested the concentrations of DEX in the injured cerebral hemisphere after intravenous injection of different doses (1 mg/kg, 5 mg, and 10 mg/kg). Consistent with previous studies, DEX was almost undetectable in the brain tissue of the low-dose group. Moreover, only a low concentration of DEX was detected in the high-dose group. Interestingly, the concentration of DEX was not significantly increased after TBI compared with the control group (Fig. 5A, B).

Local administration of MPDA@DEX@gel effectively avoided the peripheral and central side effects associated with systemic medications

In the present study, we evaluated the effect of local MPDA@DEX@gel administration on the HPA axis by testing the changes of plasma corticosterone levels after TBI. As shown in Fig. 5C, intraperitoneal administration of DEX significantly reduced the plasma corticosterone after CCI, while no statistical difference was found in plasma corticosterone between the CCI group and MPDA@DEX@gel treatment group. In addition, DEX was undetectable in both pituitary tissue and plasma in the mice of MPDA@DEX@gel treatment group. The results suggested that intraoperative local administration of DEX could effectively avoid peripheral and central side effects associated with systemic medications.

MPDA@DEX@gel restored BBB integrity, decreased BBB permeability, and reduced brain edema after TBI

In our study, we evaluated the effects of MPDA@DEX@gel on the permeability of BBB by measuring EB

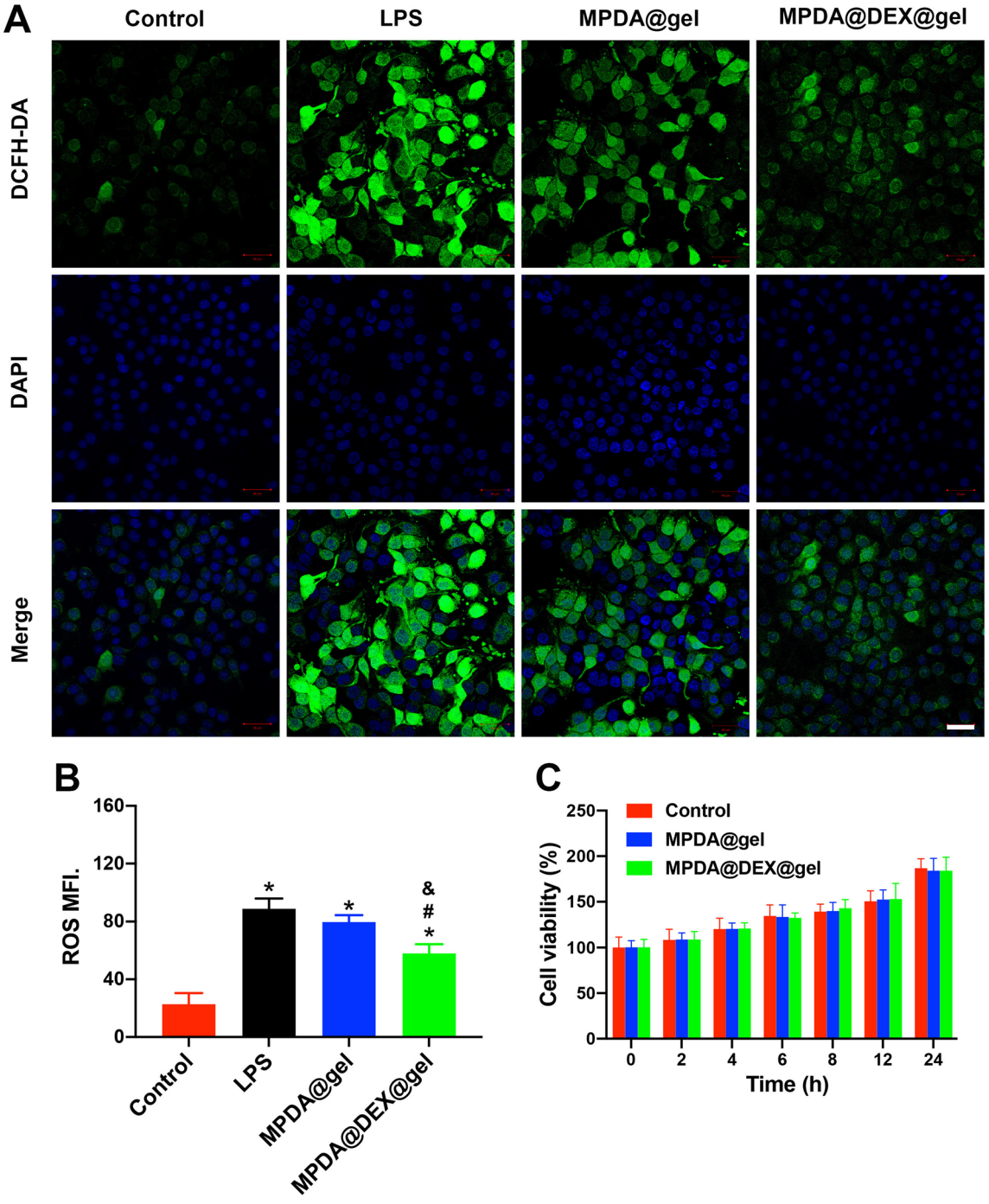

Fig. 4 Biocompatibility and antioxidant effects of different hydrogels in vitro. (**A**) Representative fluorescence images of intracellular ROS analysis with DCFH-DA (green) in LPS-stimulated BV2 cells after incubation with different hydrogels; (**B**) Semi-quantitative analysis. (Scale bar = 50 μm); (**C**) CCK-8 assay results of BV-2 after co-cultured with different leachate. *P < 0.05 compared to the control group; #P < 0.05 compared to the LPS group; &P < 0.05 compared to the MPDA@gel group. Data are presented as the means ± SDs ($n = 3$)

extravasation on postinjury day 3 after TBI. As shown in Fig. 6A-C, compared with that in the sham group, EB extravasation in the injured hemisphere was significantly increased in the CCI group, while local administration of MPDA@DEX@gel significantly reduced EB extravasation. In addition, dry/wet weight ratios were used to assess the effects of MPDA@DEX@gel on water content at 3 days after TBI (Fig. 6D). Water content in the injured hemisphere was significantly increased after TBI, whereas local administration of MPDA@DEX@gel significantly reduced EB extravasation and water content,

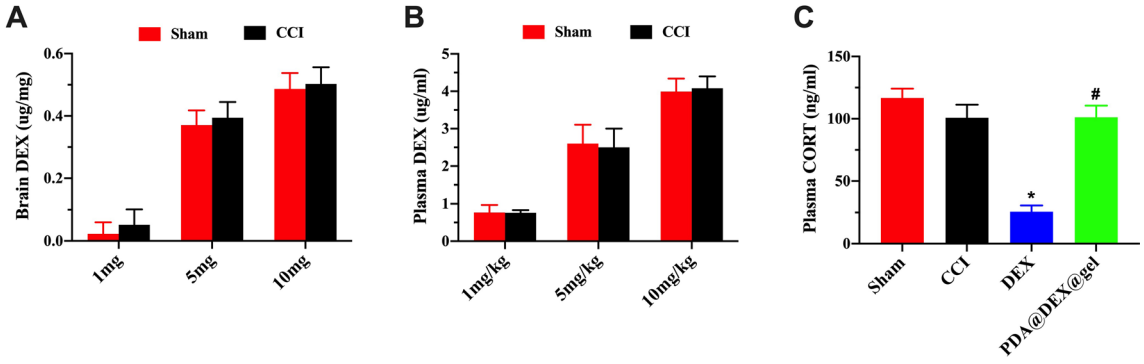

Fig. 5 The brain and plasma level of DEX and CORT after administration of DEX. (**A**) Quantification of brain tissue DEX levels in different groups after intraperitoneal administration; (**B**) Quantification of plasma DEX levels in different groups after intraperitoneal administration; (**C**) Quantification of plasma CORT levels after intraperitoneal administration and Intraoperative local administration of DEX. *P < 0.05 compared to the sham group; #P < 0.05 compared to the CCI control group. Data are presented as the means ± SDs ($n = 6$)

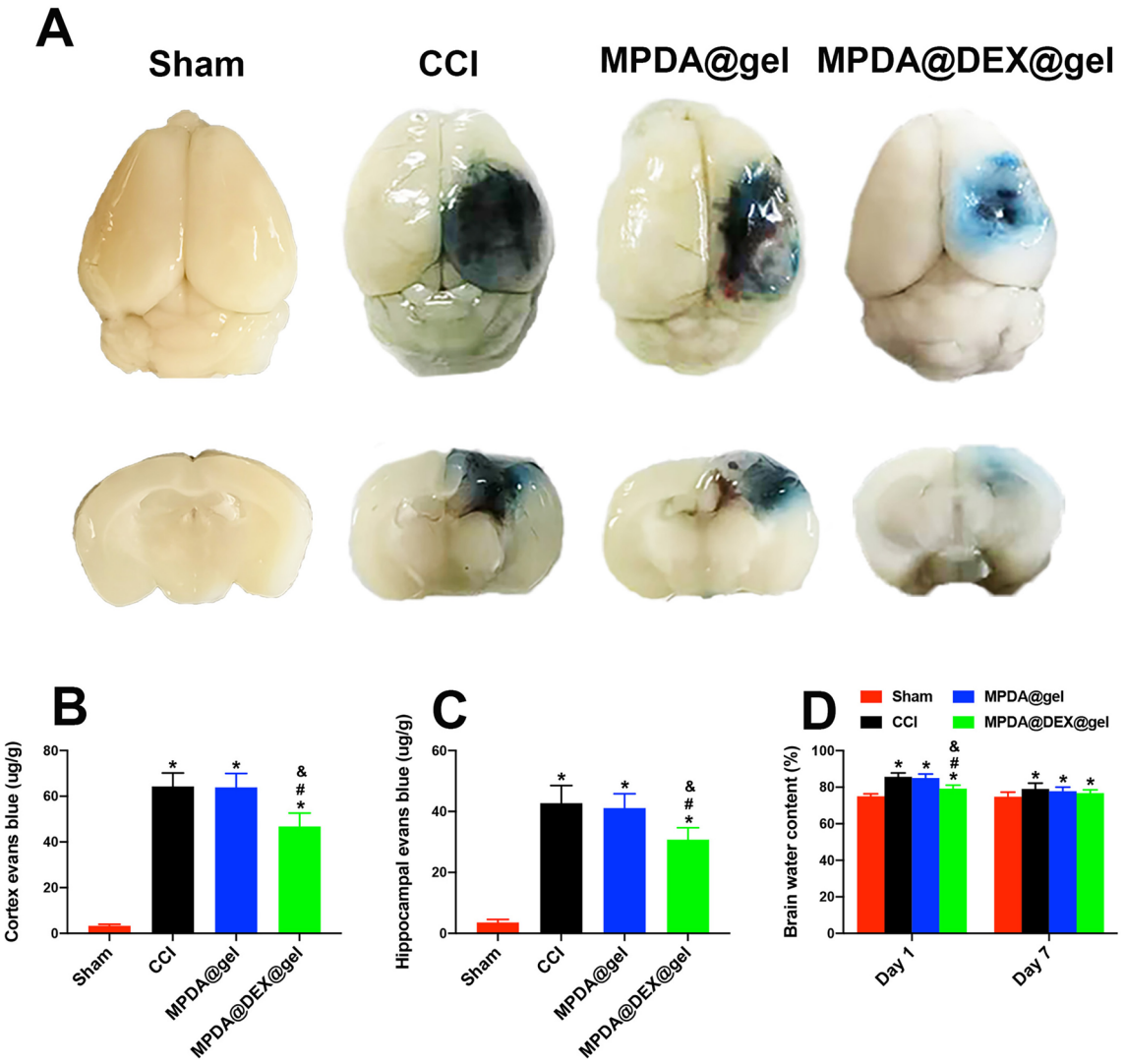

Fig. 6 Local administration of MPDA@DEX@gel restored the BBB integrity, improved the BBB permeability, and reduced brain edema at 3 days after TBI. (**A**) Representative images of Evans blue extravasation; (**B**, **C**) Quantification of EB leakage in ipsilateral cortex and hippocampus in different groups; (**D**) Quantification of brain water content in ipsilateral hemisphere in different groups. *P < 0.05 compared to the sham group; #P < 0.05 compared to the CCI control group; &P < 0.05 compared to the MPDA@gel group. The data are presented as the means ± SD ($n = 6$)

suggesting that MPDA@DEX@gel ameliorated TBI-induced damage to BBB and brain edema.

Additionally, we also examined the effects of MPDA@DEX@gel on TJ proteins after TBI, the expression levels of occludin, ZO-1 and claudin-5 were measured by western blot. As shown in Fig. 7, Occludin, ZO-1 and claudin-5 expressions were significantly reduced in the injury cortex and hippocampus 3 days after CCI. Compared with the CCI group, PMDA@DEX@Gel significantly increased the expression levels of these proteins.

MPDA@DEX@gel inhibited neuroinflammation by suppressing the activation of M1-like microglia after TBI

To evaluate the effects of MPDA@DEX@gel on neuroinflammation after TBI, we investigated the activity of proinflammatory microglia and the levels of proinflammatory cytokines in vivo and in vitro. To evaluate the effect of MPDA@DEX@gel on proinflammatory M1-like microglia, the Iba-1 + CD16/CD32 (signature markers for M1 microglia) positive cells in the injured cortex and hippocampus were counted. As shown in Fig. 8A-F, microglia was dramatically activated at 3 days after TBI, and the numbers of Iba-1CD16/CD32 positive cells were significantly increased in the injured cortex and hippocampus, while MPDA@DEX@gel treatment inhibited neuroinflammation by reducing the number of these cells.

Accordingly, the expression levels of pro-inflammatory cytokines (IL-1β, IL-6, TNF-α) in the injured cortex and hippocampus were significantly increased after TBI, while MPDA@DEX@gel treatment significantly decreased their levels (Fig. 8G-I). These results suggested that local administration of MPDA@DEX@gel effectively suppressed the inflammatory response in the brain tissue around the lesion.

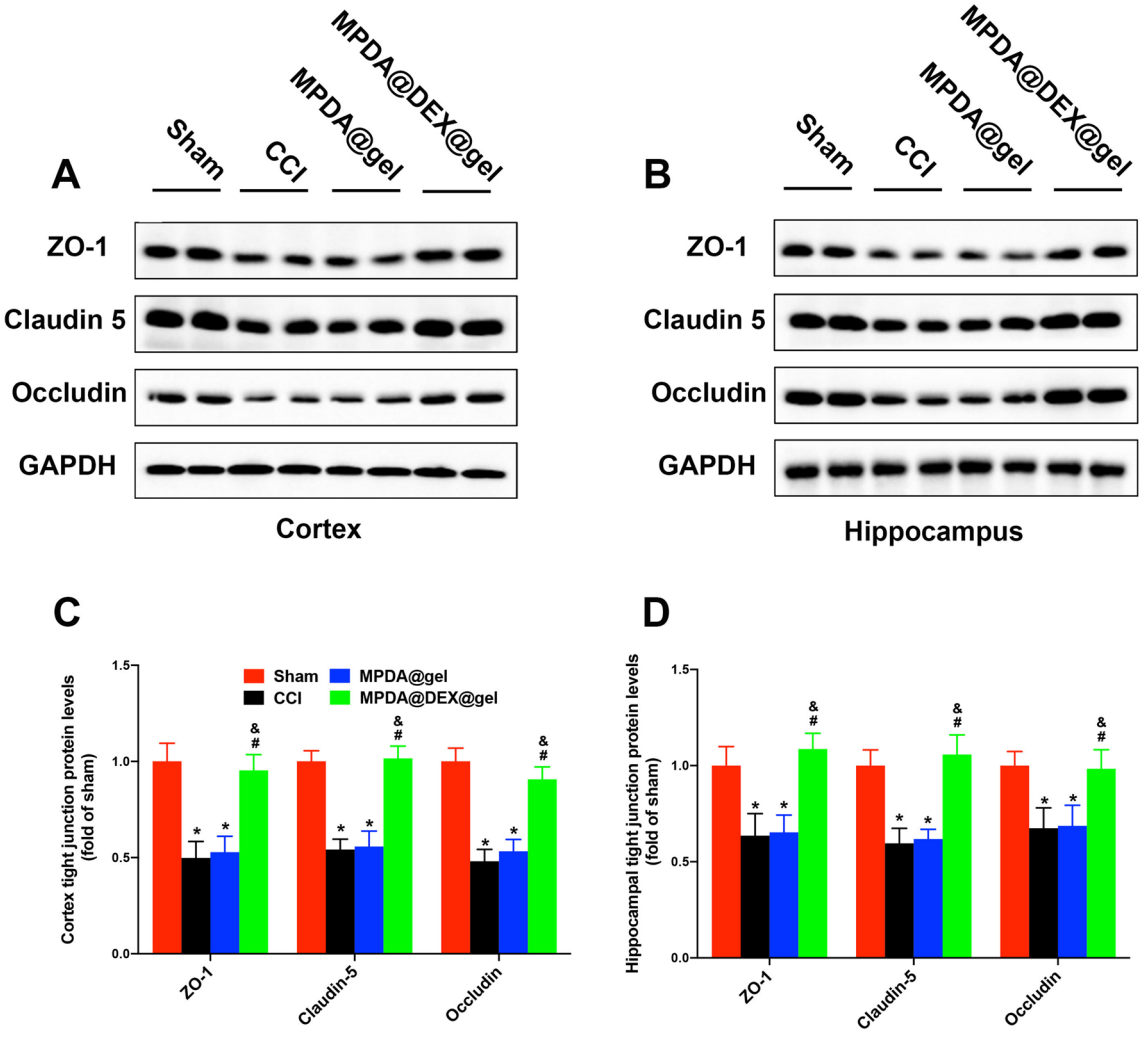

Fig. 7 Effects of Local administration of MPDA@DEX@gel on the components of BBB in the injured cortex and ipsilateral hippocampus at 3 days after TBI. (**A**, **B**) Representative images of western blot showing ZO-1, claudin-5 and occludin; (**C**, **D**) Quantification of the expressions of ZO-1, claudin-5 and occludin. *P < 0.05 compared to the sham group; #P < 0.05 compared to the CCI control group; &P < 0.05 compared to the MPDA@gel group. The data are presented as the means ± SD ($n = 6$)

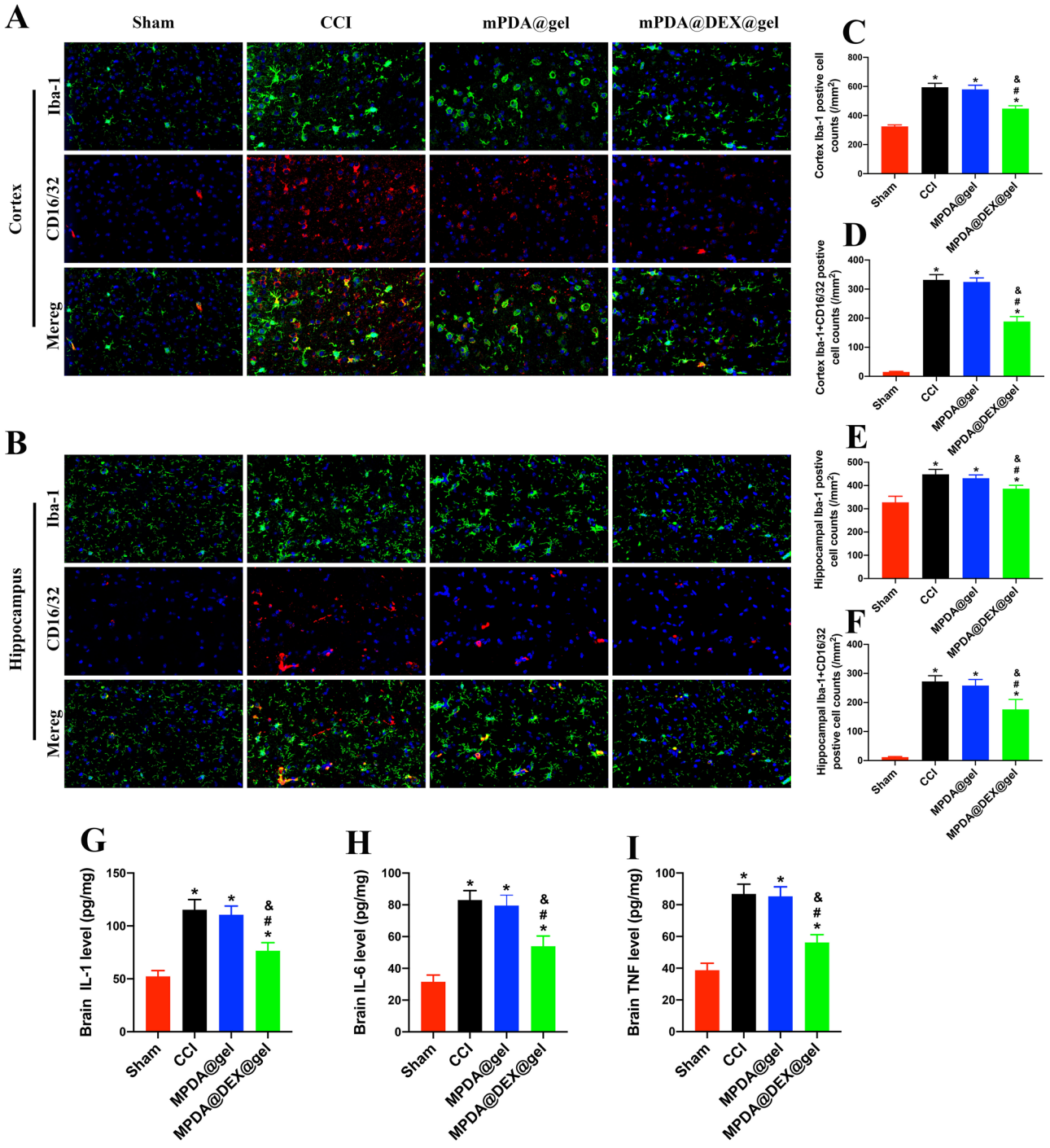

Fig. 8 Local administration of MPDA@DEX@gel inhibited neuroinflammation induced by microglia in the injured cortex and ipsilateral hippocampus after TBI (Scale bar: 100 μm). (**A**, **B**) Representative immunofluorescence images of iba- and CD16/32-positive cells; (**C**-**F**) Quantification of iba-, CD16/32; (**G**-**I**) Quantification of the inflammatory factors. *P < 0.05 compared to the sham group; #P < 0.05 compared to the CCI control group; &P < 0.05 compared to the MPDA@gel group. The data are presented as the means ± SD ($n = 6$)

MPDA@DEX@gel promoted the neuronal survival and improved neurological functions after TBI

NeuN immunofluorescence staining was conducted to assess the protective effect of MPDA@DEX@gel on neuronal survival. Our previous study showed that a continuous cell loss, which peaked at 7 days, was observed around the lesion after TBI [18]. In the present study, the number of NeuN-positive cells in both the cortex and hippocampus were significantly reduced at 7 days after CCI. In contrast, MPDA@DEX@gel treatment

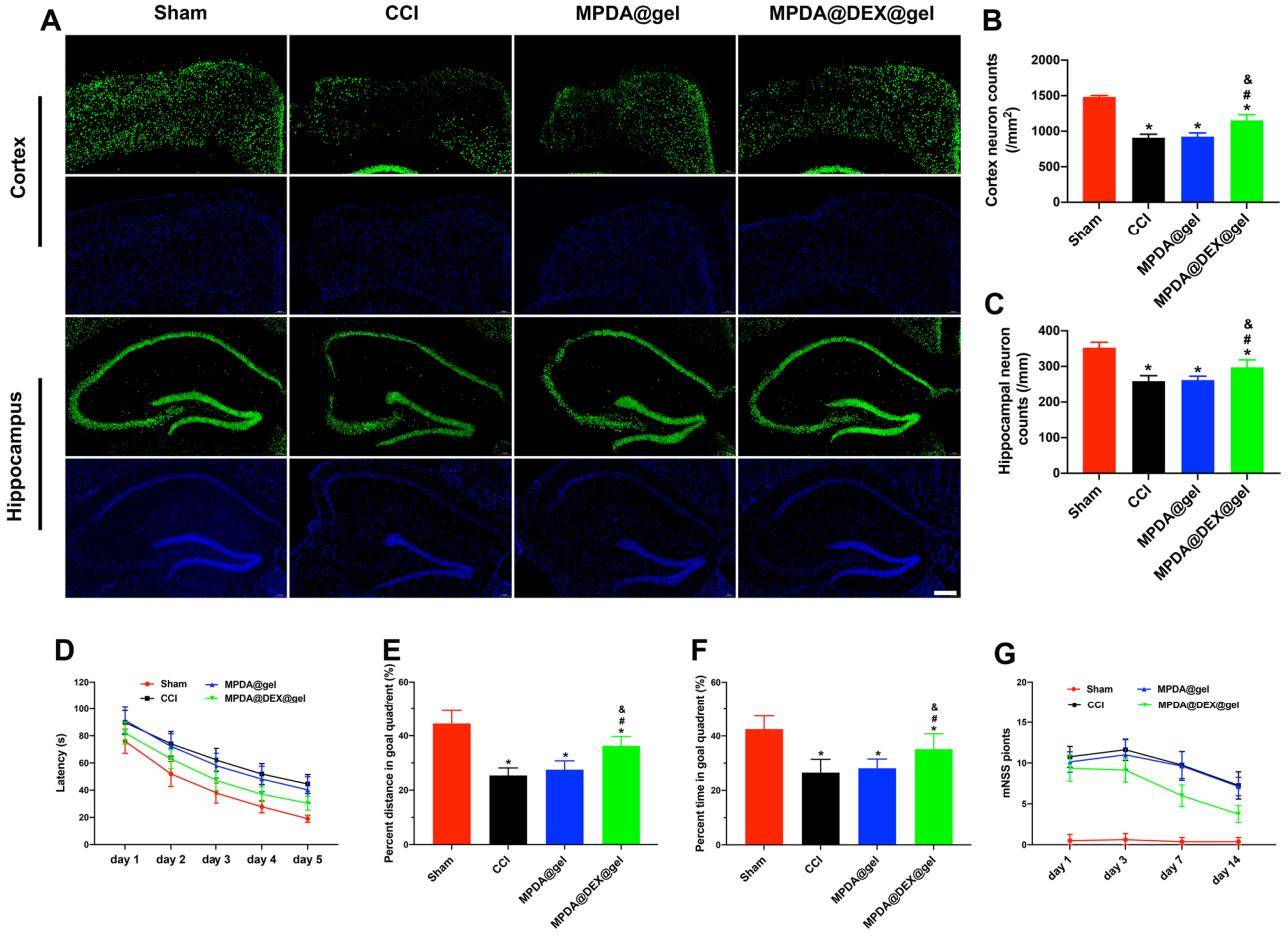

Fig. 9 Local administration of MPDA@DEX@gel promoted neuronal survival and improved neurological functions after TBI. (**A**) Representative immunofluorescence images of NEUN-positive cells in the injured cortex and ipsilateral hippocampus (Scale bar: 200 μm); (**B**, **C**) Quantification of the of NEUN-positive cells; (**D**) Quantification of the escape latency of the MWM test on days 8–12 after CCI; (**E**, **F**) Quantification of the percentage of time and distance spent in the goal quadrant during the probe trial at 13 days after CCI; (**G**) Quantification of mNSS points. *P < 0.05 compared to the sham group; #P < 0.05 compared to the CCI control group; &P < 0.05 compared to the MPDA@gel group. The data are presented as the means ± SD ($n = 6$)

significantly increased the number of NeuN-positive cells, indicating that MPDA@DEX@gel exerted neuroprotective effects (Fig. 9A-C).

The frontal and temporal lobes are the most common sites of contusion injury after TBI and are vulnerable structures to secondary injuries. CCI injury mainly induces primary focal injury in the cortex, and subsequent second injury in the pericontusion cortex and ipsilateral hippocampus, leading to the loss of neurological function, such as motor, sensory, balance, learning and memory disabilities after TBI. In the present study, The MWM and mNSS were used to evaluate neurological functions mentioned above on days 3 and 7 after TBI.

As shown in Fig. 9D-G, the escape latencies significantly increased during the trial phase after CCI, while MPDA@DEX@gel treatment significantly reduced the escape latency and improved the learning ability of the mice. In the probe trials, the percent time and distance in the goal quadrant were significantly lower in mice of the CCI group. In contrast, MPDA@DEX@gel treatment significantly increased the percentage of time and distance and improved special memory ability. In addition, the mNSS score was significantly increased at 3 and 7 days after TBI, whereas MPDA@DEX@gel treatment significantly reduced the mNSS score. The above results suggested that the administration of MPDA@DEX@gel effectively promoted the recovery of neurological function after TBI.

Discussion

In the present study, we developed an injectable nanocomposite hydrogel as a biofunctionalized delivery platform for intraoperative administration of GCs after TBI. The hydrogel is composed of CMC grafted with and OD grafted with which exhibits enhanced antibacterial and hemostatic properties. MPDA nanoparticles was added to improve the mechanical properties of the hydrogel and increase the DEX loading efficiency of hydrogel. The

MPDA@DEX@gel could realize in situ injection, self-assembly around the lesion, and exhibits excellent biocompatibility, antioxidation, and self-healing capability in vitro. By using mice CCI model, we found that local application of MPDA@DEX@gel not only inhibited neuroinflammation, alleviated brain edema, promoted neuronal survival, and improved neurological function after TBI, but also effectively avoids the peripheral and central side effects. Our study provides a promising treatment strategy for the rational use of GCs in patients with severe TBI.

The BBB plays an important role in the transmission of neuroactive agents and maintenance of fluid homeostasis [30]. Destruction of BBB structures can lead to increased permeability, enhanced neuroinflammatory responses, resulting in brain edema, intracranial hypertension, and even herniation after TBI [31]. Thus, protecting the BBB, alleviating brain edema and reducing intracranial pressure have always been the focus and challenge for TBI treatment [3]. In the early 1960s, steroids were introduced as an effective perioperative treatment for brain edema, and a clear clinical beneficial effect of steroids has been shown in patients with brain tumors, spinal cord injury, and a variety of different neurosurgical interventions [12–14]. In addition, experimental studies have revealed that steroids could inhibit neuroinflammation, protect the BBB, and reduce brain edema in animal models [32–34]. Until a favorable dose-related effect of DEX on mortality in severe TBI patients was reported, the administration of high-dose GCs including DEX and MP became commonsense for patients with severe TBI [35]. However, growing results of subsequent clinical trials did not show a substantial benefit of glucocorticoid therapy in these patients after TBI [36–38]. In contrast, the Corticosteroid Randomization After Significant Head Injury (CRASH) trial indicated that a high dose of MP was associated with increased mortality, whereas the deleterious mechanisms were unclear, and increased systemic infectious complications might be one possible mechanism [15]. In addition, previous studies revealed that a moderate amounts of synthetic glucocorticoids, such as DEX, poorly penetrates in brain because of multiple drug resistance 1a (MRDla)-encoded drug-transporting P-glycoproteins (P-gp) expressed in the apical membranes of the BBB endothelial cells, while endogenous corticosterone/cortisol can freely enter to the brain [19, 20], which might be one possible explanation for the inability of GCs to alleviate brain edema after TBI.

Among different types of GCs, synthetic glucocorticoids, especially DEX, have potent inhibitory effects on the HPA axis [39]. Previous studies have revealed that DEX mainly inhibits the activity of the HPA axis by blocking stress-induced ACTH release from the pituitary but not CRH from the hypothalamus, because dexamethasone hardly penetrates the BBB, which exists in the hypothalamus but is absent in the pituitary [40]. Therefore, DEX treatment significantly reduces the secretion of the endogenous corticosteroids but cannot fully replace the mineralocorticoid-like and glucocorticoid-like functions of endogenous corticosteroids in the brain, and eventually causes endogenous corticosteroid insufficiency and stress disorder [41]. Our previous study revealed that high-dose DEX and MP inhibited the activation of HPA axis, reduced endogenous corticosteroid level, and increased the incidence of corticosteroid insufficiency and mortality in mice after TBI [19]. Thus, the above evidence suggested that glucocorticoid-induced HPA axis dysfunction might be another important reason for the treatment failure of glucocorticoids for TBI.

Accumulating evidence have revealed that injectable hydrogel is an ideal supporting matrix and drug delivery platforms to realize local drug application and promote brain tissue repair after TBI [23–25]. Therefore, we speculated that intraoperative local administration of DEX by using hydrogel might be a rational way of GCs administration for severe TBI patients requiring surgery. Compared with synthetic polymers, polysaccharides, such as dextran and chitosan, are excellent natural hydrogel materials because of their superior biodegradability, biocompatibility and improved safety profile for clinical application [42–45]. Chitosan and oxidized dextran can cross-link and form self-healing hydrogel via an aldehyde-amine Schiff-base reaction. The gelation process is rapid and gentle, providing an excellent raw material for in situ injectable hydrogel. In addition, chitosan and dextran can be easily modified to improve their intrinsic properties, such as their water solubility and antiseptic and hemostatic properties [46]. However, the low mechanical strength, low drug-loading rate and uncontrolled burst release, weak controllability and other disadvantages of conventional hydrogels limit their applications. Therefore, less hydrogels are clinically applied in brain.

MPDA NPs were formed by self-assembly of dopamine via π-π stacking interactions in ethanol and ammonia solution. Compared with PDA, the surface area and drug release time of MPDA NPs and other mesoporous NPs are dramatically increased [47]. Therefore, MPDA nanoparticles is a more ideal drug carrier owing to their high drug-load ratio, good biocompatibility and biodegradability [48–50]. Dexamethasone contains conjugated double bonds and is hydrophobic. Because of their large number of phenolic hydroxyl groups, such as amino, benzene ring, carbonyl group, MPDA nanoparticles can absorb DEX via hydrophobic interaction, π-π conjugation, electrostatic interaction, van der Waals force, and hydrogen bonding. To avoid the shortcomings and improve the therapeutic effects of hydrogel, we

developed an injectable nanocomposite hydrogel by adding MPDA to hydrogel for intraoperative administration of DEX after TBI. The hydrogel is composed of polysaccharide matrix (CMC and OD) and MPDA nanoparticles loaded with DEX (MPDA@DEX@gel). In addition, antiseptic quaternary ammonium salt (EPD) and hemostatic polypeptide (RAD-OD) were grafted to CMC and RAD respectively to enhance the antibacterial and hemostatic properties of the hydrogel. Our results revealed that DEX in the blank hydrogel was released rapidly in the first few hours, whereas MPDA@DEX@gel exhibited a high DEX loading rate and realized a continuous and controlled release of DEX. MPDA@DEX@gel possessed excellent antibacterial and hemostatic properties, good biocompatibility and antioxidation, injectability and self-healing capability in vitro. In addition, the volume of the wet hydrogel did not continue to increase after local administration and would not cause mass effect that compressed the surrounding brain tissue. The addition of MPDA enhanced the mechanical strength and the thermal stability of the hydrogel by increasing the number of Schiff-base reaction sites and promoted the internal cross-linking of the hydrogel. The hydrogel can firmly adhere to the fresh brain and resist the water scouring.

Accordingly, our results showed that DEX poorly penetrated BBB and were almost undetectable after intravenous injection of low and moderate doses of DEX. Even with the dose up to 10 mg/kg, only a low concentration of DEX was detected in the brain. Not as expected, TBI did not significantly increase the dexamethasone level in the injured hemisphere, the mechanism remained unclear, which may be partly due to focal vascular injuries, reduced local cerebral blood flow, hypoxia-ischemia, brain edema, and increased ICP. In contrast, For the mice in the MPDA@DEX@gel group, 50 μL of hydrogel containing 25ug DEX were injected in situ into the surgical area. Previous experimental studies used 10 mg/kg DEX as a high dose for systemic administration after TBI model [28]. In the present study, each mouse (about 25 g) received approximately 250 ug of DEX via intraperitoneal administration, and this dose was about ten folds that of local administration, while the local DEX concentration was much lower than local administration. The results suggested that intraoperative local administration of DEX could effectively circumvent the BBB, release DEX directly to the focal injury site, increase the local drug concentration, and enhance its therapeutic effects. In addition, systemic administration of DEX inhibited the activity of HPA axis, subsequently reduced the plasma corticosterone after TBI, whereas local MPDA@DEX@gel administration did not affect the HPA axis and plasma corticosterone. Moreover, DEX was undetectable in both pituitary tissue and plasma in the mice of MPDA@DEX@gel treatment group. The results suggested that intraoperative local administration of DEX could effectively avoid peripheral and central side effects associated with systemic medications.

Besides primary injury by direct mechanical force, the integrity of BBB can also be affected by secondary injury mechanisms, especially neuroinflammation. Both peripheral and innate immune cells are involved in acute neuroinflammatory responses after TBI [51, 52]. Microglia, as the major resident immune cells in the brain, serve as the first line of defense against injuries, and immediately initiate a cascade of inflammatory response after initial mechanical damage to the brain occurs after TBI. In addition, astrocytes surrounding the injured region are activated by cell debris and inflammatory cytokines, which in turn produce inflammatory cytokines and activate the surveillance microglia. By releasing proinflammatory cytokines and increasing the permeability of the BBB, microglia can recruit peripheral phagocytes into the brain via a damaged BBB. In particular, interleukin (IL)-1β, IL-6, and tumor necrosis factor-α (TNF-α), are the most important proinflammatory cytokines that exacerbate and increase BBB permeability [53, 54]. Therefore, we investigated the anti-inflammatory effects of MPDA@DEX@gel by testing the activities of the proinflammatory microglia and the levels of proinflammatory cytokines around the lesion after TBI. Results from in vivo TBI mice model revealed that the proinflammatory types of microglia dramatically proliferated and the expression levels of proinflammatory cytokines were increased around the lesion, whereas local application of MPDA@DEX@gel exerted potent anti-inflammatory effects by inhibiting the activated microglia and astrocytes as well as the release of proinflammatory cytokines. The above results indicated that MPDA@DEX@gel protected the BBB and reduced brain edema, possibly through blocking neuroinflammation mediated by proinflammatory cells after TBI.

Moreover, NeuN immunofluorescence staining revealed that MPDA@DEX@gel treatment exerted neuroprotective effects and promoted the survival of neurons around the lesion after TBI. The results of mNSS and MWM showed that MPDA@DEX@gel improved the recovery of neurological function after TBI. The above results suggest that local MPDA@DEX@gel application protected the BBB, reduced brain edema, and subsequently promoted the survival of neurons and improved the neurological function by alleviating neuroinflammation after TBI.

Conclusion

In summary, we developed an injectable nanoarchitecture-integrated hydrogel delivery nanoplatform for the intraoperative local administration of DEX after TBI. CMC and OD gelatinized in situ fast and mildly via an

aldehyde-amine Schiff-base reaction and filled the irregular lesion cavities in the injured brain. The hydrogel exhibited excellent antibacterial and hemostatic properties by grafting with antiseptic quaternary ammonium salt and hemostatic polypeptides. MPDA NPs dramatically increased the DEX loading capacity of the hydrogel and enhanced the retention time of loaded DEX. The MPDA NPs were highly dispersed in the hydrogels. Therefore, intraoperative administration of MPDA@DEX@gel realized sustained release of DEX, leading to a high level of DEX in brain tissue around the lesion for several days. These in vitro and in vivo results revealed that local application of MPDA@DEX@gel not only alleviated brain edema, promoted neuronal survival, and improved neurological function by restoring the integrity of BBB, reducing the permeability of BBB, and inhibiting neuroinflammation, but also effectively avoided the peripheral and central side effects. Overall, our study revealed the possible mechanisms for the failure of systemic application of GCs in patients with severe TBI and presented a MPDA@DEX@gel that offered a promising and rational administration strategy of GCs for TBI.

Abbreviations

ACTH	Adrenocorticotropic hormone
BBB	Blood-brain barrier
CCI	Controlled cortical impact
CMC	Carboxymethyl chitosan
CRASH	Corticosteroid Randomization After Significant Head Injury
CRH	Corticotrophin-releasing hormone
DEX	Dexamethasone
E. coli	Escherichia coli
EB	Evans blue
GCs	Glucocorticoids
HPA	Hypothalamic-pituitary-adrenal
ICP	Increased intracranial pressure
mNSS	Modified neurological severity score
MP	Methylprednisolone
MPDA	Mesoporous polydopamine
MRDIa	Multiple drug resistance 1a
MRI	Magnetic Resonance Imaging
MWM	Morris water maze
OD	Oxidized dextran
P-gp	P-glycoproteins
PVN	Paraventricular hypothalamic nucleus
S. aureus	Staphylococcus aureus
TBI	Traumatic brain injury

Supplementary Information

The online version contains supplementary material available at https://doi.org/10.1186/s12967-025-06528-w.

Supplementary Material 1

Acknowledgements

We thank the Beijing neurosurgical institute consultation and instrument availability that supported this work. The authors would like to acknowledge the efforts of all the staff who contributed to this study.

Author contributions

GS and BZ conceived and designed the experiments. BZ, MB, YW, MY, and XC performed experiments. BZ and MB provided input on data analysis and computational approaches. BZ, MB, and BL wrote and revised the manuscript. All authors read and approved the final manuscript.

Funding

This work was partially supported by Beijing Science and Technology Planning Project (CN) (Z201100005520039) and Natural Science Foundation of Capital Medical University (PYZ23123).

Data availability

The datasets used and/or analyzed during the current study are available from the corresponding author on reasonable request.

Declarations

Ethics approval

The experiments were approved by the Capital Medical University Institutional Animal Care and Use Committee.

Competing interests

The authors declare no competing interests.

Received: 16 March 2025 / Accepted: 22 April 2025
Published online: 23 May 2025

References

1. Wilson L, Stewart W, Dams-O'Connor K, Diaz-Arrastia R, Horton L, Menon DK, et al. The chronic and evolving neurological consequences of traumatic brain injury. Lancet Neurol. 2017;16:813–25.
2. Maas A, Menon DK, Manley GT, Abrams M, Akerlund C, Andelic N, et al. Traumatic brain injury: progress and challenges in prevention, clinical care, and research. Lancet Neurol. 2022;21:1004–60.
3. Sulhan S, Lyon KA, Shapiro LA, Huang JH. Neuroinflammation and blood-brain barrier disruption following traumatic brain injury: pathophysiology and potential therapeutic targets. J Neurosci Res. 2020;98:19–28.
4. Marmarou A. Traumatic brain edema: an overview. Acta Neurochir Suppl (Wien). 1994;60:421–4.
5. Stocchetti N, Maas AI. Traumatic intracranial hypertension. N Engl J Med. 2014;370:2121–30.
6. van Hameren G, Aboghazleh R, Parker E, Dreier JP, Kaufer D, Friedman A. From spreading depolarization to blood–brain barrier dysfunction: navigating traumatic brain injury for novel diagnosis and therapy. Nat Reviews Neurol. 2024;20:408–25.
7. Winkler EA, Minter D, Yue JK, Manley GT. Cerebral edema in traumatic brain injury. Neurosurg Clin N Am. 2016;27:473–88.
8. Hutchinson PJ, Kolias AG, Timofeev IS, Corteen EA, Czosnyka M, Timothy J, et al. Trial of decompressive craniectomy for traumatic intracranial hypertension. N Engl J Med. 2016;375:1119–30.
9. Liu J, Liu H, Huang S, Peng H, Li J, Tu K, et al. Multiple treatment of Triple-Negative breast Cancer through gambogic Acid-Loaded mesoporous polydopamine. Small. 2024;20:e2309583.
10. Harris WJ, Asselin M, Hinz R, Parkes LM, Allan S, Schiessl I, et al. In vivo methods for imaging blood–brain barrier function and dysfunction. Eur J Nucl Med Mol Imaging. 2023;50:1051–83.
11. Pan J, Wang Z, Huang X, Xue J, Zhang S, Guo X, et al. Bacteria-Derived Outer-Membrane vesicles hitchhike neutrophils to enhance ischemic stroke therapy. Adv Mater (Weinheim). 2023;35:e2301779.
12. Renaudin J, Fewer D, Wilson CB, Boldrey EB, Calogero J, Enot KJ. Dose dependency of decadron in patients with partially excised brain tumors. J Neurosurg. 1973;39:302–5.
13. Reichardt HM, Gold R, Luhder F. Glucocorticoids in multiple sclerosis and experimental autoimmune encephalomyelitis. Expert Rev Neurother. 2006;6:1657–70.
14. Bracken MB, Shepard MJ, Collins WF, Holford TR, Young W, Baskin DS, et al. A randomized, controlled trial of Methylprednisolone or Naloxone in the treatment of acute spinal-cord injury. Results of the second National acute spinal cord injury study. N Engl J Med. 1990;322:1405–11.
15. Edwards P, Arango M, Balica L, Cottingham R, El-Sayed H, Farrell B, et al. Final results of MRC CRASH, a randomised placebo-controlled trial of intravenous

corticosteroid in adults with head injury-outcomes at 6 months. Lancet. 2005;365:1957–9.
16. Saul TG, Ducker TB, Salcman M, Carro E. Steroids in severe head injury: A prospective randomized clinical trial. J Neurosurg. 1981;54:596–600.
17. Zhang B, Bai M, Xu X, Yang M, Niu F, Gao F, et al. Corticosteroid receptor rebalancing alleviates critical illness-related corticosteroid insufficiency after traumatic brain injury by promoting paraventricular nuclear cell survival via Akt/CREB/BDNF signaling. J Neuroinflammation. 2020;17:318.
18. Zhang B, Xu X, Niu F, Mao X, Dong J, Yang M, et al. Corticosterone replacement alleviates hippocampal neuronal apoptosis and Spatial memory impairment induced by dexamethasone via promoting brain corticosteroid receptor rebalance after traumatic brain injury. J Neurotrauma. 2020;37:262–72.
19. Mason BL, Pariante CM, Thomas SA. A revised role for P-Glycoprotein in the brain distribution of dexamethasone, cortisol, and corticosterone in Wild-Type and ABCB1A/B-Deficient mice. Endocrinology. 2008;149:5244–53.
20. De Kloet ER. Why dexamethasone poorly penetrates in brain. Stress. 1997;2:13–20.
21. Shan BH, Wu FG. Hydrogel-Based growth factor delivery platforms: strategies and recent advances. Adv Mater. 2024;36:e2210707.
22. Correa S, Grosskopf AK, Lopez Hernandez H, Chan D, Yu AC, Stapleton LM, et al. Translational applications of hydrogels. Chem Rev. 2021;121:11385–457.
23. Kumar PA, Mohamed MA, Seidman RA, Tseropoulos G, Polanco JJ, Lei P, et al. Injectable shear-thinning hydrogels promote oligodendrocyte progenitor cell survival and remyelination in the central nervous system. Sci Adv. 2024;10:eadk9918.
24. Han Y, Weng W, Zhang Y, Feng Q, Ma Y, Quan A, et al. Intraoperative application of intelligent, responsive, self-assembling hydrogel rectifies oxygen and energy metabolism in traumatically injured brain. Biomaterials. 2024;306:122495.
25. Ma X, Agas A, Siddiqui Z, Kim K, Iglesias-Montoro P, Kalluru J, et al. Angiogenic peptide hydrogels for treatment of traumatic brain injury. Bioact Mater. 2020;5:124–32.
26. Griffith LG, Swartz MA. Capturing complex 3D tissue physiology in vitro. Nat Rev Mol Cell Biol. 2006;7:211–24.
27. Eelkema R, Pich A. Pros and cons: supramolecular or macromolecular: what is best for functional hydrogels with advanced properties? Adv Sci (Weinh). 2020;32:e1906012.
28. Ding C, Liu X, Zhang S, Sun S, Yang J, Chai G, et al. Multifunctional hydrogel bioscaffolds based on polysaccharide to promote wound healing: A review. Int J Biol Macromol. 2024;259:129356.
29. Zhu H, Zheng J, Oh XY, Chan CY, Low B, Tor JQ, et al. Nanoarchitecture-Integrated hydrogel systems toward therapeutic applications. ACS Nano. 2023;17:7953–78.
30. Zhao Z, Nelson AR, Betsholtz C, Zlokovic BV. Establishment and dysfunction of the Blood-Brain barrier. Cell. 2015;163:1064–78.
31. van Vliet EA, Ndode-Ekane XE, Lehto LJ, Gorter JA, Andrade P, Aronica E, et al. Long-lasting blood-brain barrier dysfunction and neuroinflammation after traumatic brain injury. Neurobiol Dis. 2020;145:105080.
32. Maxwell RE, Long DM, French LA. The effects of glucosteroids on experimental cold-induced brain edema. Gross morphological alterations and vascular permeability changes. J Neurosurg. 1971;34:477–87.
33. Dick AR, McCallum ME, Maxwell JA, Nelson R. Effect of dexamethasone on experimental brain edema in cats. J Neurosurg. 1976;45:141–7.
34. Hall ED. The neuroprotective Pharmacology of Methylprednisolone. J Neurosurg. 1992;76:13–22.
35. Gobiet W, Bock WJ, Liesgang J. Treatment of acute cerebral edema with high dose of dexamethasone. In: Beks JWF, Bosch DA, Brock M, editors. Intracranial pressure III. New York: Springer-; 1976. pp. 231–5.
36. Dearden NM, Gibson JS, McDowall DG, Gibson RM, Cameron MM. Effect of high-dose dexamethasone on outcome from severe head injury. J Neurosurg. 1986;64:81–8.
37. Giannotta SL, Weiss MH, Apuzzo ML, Martin E. High dose glucocorticoids in the management of severe head injury. Neurosurgery. 1984;15:497–501.
38. Gudeman SK, Miller JD, Becker DP. Failure of high-dose steroid therapy to influence intracranial pressure in patients with severe head injury. J Neurosurg. 1979;51:301–6.
39. de Kloet ER. Glucocorticoid feedback paradox: a homage to Mary Dallman. Stress. 2023;26:2247090.
40. de Kloet ER, van der Vies J, de Wied D. The site of the suppressive action of dexamethasone on pituitary-adrenal activity. Endocrinology. 1974;94:61–73.
41. de Kloet ER. Brain mineralocorticoid and glucocorticoid receptor balance in neuroendocrine regulation and stress-related psychiatric etiopathologies. Curr Opin Endocr Metab Res. 2022;24:100352.
42. Ji X, Shao H, Li X, Ullah MW, Luo G, Xu Z, et al. Injectable immunomodulation-based porous Chitosan microspheres/hpch hydrogel composites as a controlled drug delivery system for osteochondral regeneration. Biomaterials. 2022;285:121530.
43. Meng J, Yang X, Huang J, Tuo Z, Hu Y, Liao Z et al. Ferroptosis-Enhanced immunotherapy with an injectable Dextran-Chitosan hydrogel for the treatment of malignant Ascites in hepatocellular carcinoma. Adv Sci (Weinh). 2023;10(20):e2300517.
44. Huang Y, Mu L, Zhao X, Han Y, Guo B. Bacterial Growth-Induced tobramycin smart release Self-Healing hydrogel for Pseudomonas aeruginosa-Infected burn wound healing. ACS Nano. 2022;16:13022–36.
45. Zhang A, Cong L, Nan C, Zhao Z, Liu L. 3D biological scaffold delivers Bergenin to reduce neuroinflammation in rats with cerebral hemorrhage. J Transl Med. 2024;17;22(1):946.
46. Zhao X, Wu H, Guo B, Dong R, Qiu Y, Ma PX. Antibacterial anti-oxidant electroactive injectable hydrogel as self-healing wound dressing with hemostasis and adhesiveness for cutaneous wound healing. Biomaterials. 2017;122:34–47.
47. Arvejeh PM, Chermahini FA, Marincola F, Taheri F, Mirzaei SA, Alizadeh A et al. A novel approach for the co-delivery of 5-fluorouracil and everolimus for breast cancer combination therapy: stimuli-responsive chitosan hydrogel embedded with mesoporous silica nanoparticles. J Transl Med. 2025; 31;23(1):382.
48. Yang J, Wang M, Zheng S, Huang R, Wen G, Zhou P, et al. Mesoporous polydopamine delivering 8-gingerol for the target and synergistic treatment to the spinal cord injury. J Nanobiotechnol. 2023;21:192.
49. Park J, Brust TF, Lee HJ, Lee SC, Watts VJ, Yeo Y. Polydopamine-based simple and versatile surface modification of polymeric nano drug carriers. ACS Nano. 2014;8:3347–56.
50. Deng Q, Gao Y, Rui B, Li X, Liu P, Han Z, et al. Double-network hydrogel enhanced by SS31-loaded mesoporous polydopamine nanoparticles: symphonic collaboration of near-infrared photothermal antibacterial effect and mitochondrial maintenance for full-thickness wound healing in diabetes mellitus. Bioact Mater. 2023;27:409–28.
51. Morganti-Kossmann MC, Semple BD, Hellewell SC, Bye N, Ziebell JM. The complexity of neuroinflammation consequent to traumatic brain injury: from research evidence to potential treatments. Acta Neuropathol. 2019;137:731–55.
52. Hu X, Leak RK, Shi Y, Suenaga J, Gao Y, Zheng P, et al. Microglial and macrophage polarization-new prospects for brain repair. Nat Rev Neurol. 2015;11:56–64.
53. Li Y, Ren X, Zhang L, Wang Y, Chen T. Microglial polarization in TBI: signaling pathways and influencing pharmaceuticals. Front Aging Neurosci. 2022;14:901117.
54. Huang T, Wu J, Mu J, Gao J. Advanced therapies for traumatic central nervous system injury: delivery strategy reinforced efficient microglial manipulation. Mol Pharm. 2023;20:41–56.

Publisher's note

Springer Nature remains neutral with regard to jurisdictional claims in published maps and institutional affiliations.